IEEE Access
Multidisciplinary | Rapid Review | Open Access Journal

Received October 15, 2020, accepted November 1, 2020, date of publication November 4, 2020, date of current version November 19, 2020.

Digital Object Identifier 10.1109/ACCESS.2020.3035905

Voltage and Current Measuring Technologies for High Voltage Direct Current Supergrids: A Technology Review Identifying the Options for Protection, Fault Location and Automation Applications

DIMITRIOS TZELEPIS[1], (Member, IEEE), VASILEIOS PSARAS[1], (Student Member, IEEE), ELENI TSOTSOPOULOU[1], (Student Member, IEEE), SOHRAB MIRSAEIDI[2], (Member, IEEE), ADAM DYŚKO[1], (Member, IEEE), QITENG HONG[1],(Member, IEEE), XINZHOU DONG[3], (Fellow, IEEE), STEVEN M. BLAIR[1,4], (Senior Member, IEEE), VASSILIS C. NIKOLAIDIS[5], (Senior Member, IEEE), VASSILIS PAPASPILIOTOPOULOS[6], (Member, IEEE), GRZEGORZ FUSIEK[1], (Member, IEEE), GRAEME M. BURT[1], (Member, IEEE), PAWEL NIEWCZAS[1,4], (Member, IEEE), AND CAMPBELL D. BOOTH[1,4], (Member, IEEE)

[1]Department of Electronics & Electrical Engineering, University of Strathclyde, Glasgow G1 1XQ, U.K.
[2]School of Electrical Engineering, Beijing Jiaotong University, Beijing 100044, China
[3]Department of Electrical Engineering, Tsingua University, Beijing 100084, China
[4]Synaptec Ltd., Glasgow G1 1XW, U.K.
[5]Department of Electrical and Computer Engineering, Democritus University of Thrace, 67100 Xanthi, Greece
[6]PROTASIS SA, 15231 Athens, Greece

Corresponding author: Dimitrios Tzelepis (dimitrios.tzelepis@strath.ac.uk)

This work was supported in part by The Royal Society of Edinburgh (J. M. Lessells Scholarship), in part by the PHOENIX Project U.K., under Grant SPTEN03, in part by the Innovate U.K. under Project 102594 and Project 109487-627607, in part by the U.K. Engineering and Physical Sciences Research Council under Grant EP/P510300/1, and in part by the National Key Research and Development Plan of China under Grant 2018YFB0904602.

ABSTRACT After the occurrence of a DC-side feeder faults on HVDC transmission systems, protection and fault detection systems are anticipated to minimize their onerous effects, by initiating fault-clearing actions such as selective tripping of circuit breakers. Following the successful fault clearance, a subsequent action of significant importance, is the meticulous estimation of its location as a means to accelerate the line restoration, reduce down-time, limit recovery and repair costs, and hence elevate the overall availability and reliability of the transmission system. In order to capture DC-side fault transients for protection and fault location applications, measuring equipment is required to be placed on HVDC installations. This paper focuses primarily on reviewing the available technologies from the perspective of enabling protection, fault location and automation applications in HVDC systems. The review constitutes a mapping of protection and fault location functions, against the available voltage and current measuring technologies, ultimately unlocking insights for selecting measuring equipment based on the desirable characteristics of protection and fault location systems. The review also revealed that the frequency characteristics of each sensing scheme, primarily refers to the bandwidth of the primary sensor, whereas the overall bandwidth of the complete measuring scheme may be further restricted by the secondary converter and corresponding data acquisition system and signal processing electronics. It was also identified that the use of RC voltage dividers has prevailed for voltage measurements for HVDC applications, due to their superior advantages. The choice of a suitable device for current measurement, depends mainly on the fault detection method used and the frequency range it operates. In particular, the review revealed that fault detection and protection methods are mainly concentrated in a frequency spectrum ranging from a few kHz to 100 kHz, while fault location methods require measurements with a frequency range from 100 kHz up to 2 MHz.

INDEX TERMS HVDC technology, fault detection, fault location, power system measurements.

The associate editor coordinating the review of this manuscript and approving it for publication was Dazhong Ma.

NOMENCLATURE

$1D-CNN$	One-Dimensional Convolutional Neural Network
Δi	Differential Current
Δv	Differential Voltage
$\int V_{Ldc}$	Integral of DC reactor voltage
∇v	voltage gradient
$\rho(d,x)$	Pearson's correlation coefficient
ATTW	Arrival Time of Traveling Waves
BGO	Bismuth Germanium Oxide
CLRP	Current Limiting Reactor Power
ConvoP	Convolution of Power
CovoI	Covariance of Current
CPTE	Convolution Power-based Transient Energy
CRP	Current Reduction Phenomenon
CS	Cosine Distance
CSoTW	Cosine Similarity of Travelling Waves
CWT	Continuous Wavelet Transform
$d(i/v)/dt$	Rate of change of current-voltage ratio
$d\bar{I}$	Deviation of current from its moving average
di/dt	Rate of change of current
DiroI	Direction of Current
DNF	Dominant Natural Frequency
dv/dt	Rate of change of voltage
DVTW	Differential Voltage Travelling Wave
DWT	Discrete Wavelet Transform
$DWT(i)$	Discrete Wavelet Transform of Current
$DWT(v)$	Discrete Wavelet Transform of Voltage
EEMD	Ensemble Empirical Mode Decomposition
EMD	Empirical Mode Decomposition
EML	Extreme Machine Learning
EMTR	Electro-Magnetic Time Reversal
$fit(i)$	Time-domain fitting of fault current
FLC	Fault Location Coefficient
FPT	First Peak Time
FSC	Frequency Spectrum Correlation
GFS	Generic Fuzzy System
GTBL	Graph Theory-Based Lemmas
HFTVE	High Frequency Transient-Voltage Energy
HHT	Hilbert–Huang Transform
HVDC	High Voltage Direct Current
IED	Intelligent Electronic Device
LCC	Line Commutated Converters
LPCT	Low Power Current Transformers
LPIT	Low Power Instrument Transformers
LPVT	Low Power Voltage Transformers
MAD	Median Absolute Value
MMC	Modular Multi-level Converters
ModVel	Modal Velocities
MTDC	Mutli Terminal Direct Current
MVVDF	Minimum Value of Voltage Distribution Functions
NBC	Nave Bayer Classifier
OC	Over-Current
OHL	Over-Head Lines
OV	Over-Voltage
PCA	Principal Component Analysis
PCC	Pearson's Correlation Coefficients
PTG	Pole-To-Ground
PTP	Pole-To-Pole
QCD	Quickest Change Detection
RES	Renewable Energy Sources
ROHTLFC	Ratio Of High-To-Low-Frequency Currents
ROTV	Ratio of Transient Voltages
$RT-BWT$	Real-Time Boundary Wavelet Transform
SATD	Surge Arrival Time Difference
$sgn(di/dt)$	Sign/polarity of current derivative
$sgn(dv/dt)$	Sign/polarity of voltage derivative
$sgn(i)$	Sign/polarity of current
$sgn(WTMM)$	Sign/polarity of Wavelet Transform Modulus Maxima
SMVS	Simularity Measure of Voltage Signals
SVM	Support Vector Machines
SWT	Stationary Wavelet Transform
TER	Ratio of Transient Energy
THFE	Transient High-Frequency Energy
TVAC	Transient Average Value of Current
TVE	Transient Voltage Energy
TWFSR	Travelling Wave Frequency Spectrum Analysis
TWD	Travelling Wave Differential
UV	Under-Voltage
VCI	Voltage Change Integral
VPI	Voltage Pulse Injection
WAF	Weughted Averaging Functions
WCoV	Wavelet Coefficients of Voltage
$WE(i)$	Wavelet Energy of Current
$WER(i)$	Wavelet Energy Ratios of Current
WPEE	Wavelet-Packet Energy Entropy
WT	Wavelet Transform
WTMM	Wavel Transform Modulus Maxima
$WTMM(i)$	Wavelet Transform Modulus Maxima current

I. INTRODUCTION

Due to the high penetration of Renewable Energy Sources (RES), demand and supply equilibrium is anticipated to be one of the key challenges in future operation of power systems. Consequently, there is an emerging need for meshed interlinks between different countries as a means to efficiently exchange the available energy and therefore increase the flexibility and security of supply.

The concept of supergrid has been identified as a possible mechanism towards a new backbone transmission system, allowing massive integration of RES [1]–[5]. High Voltage Direct Current (HVDC) links, utilizing Voltage Source Con-

verters (VSCs), are expected to become the favourable technology for realization of such a supergrid [6]. This is driven by the fact that such systems are characterized by superior features in terms of operational losses, system stability and cost.

An extension of existing HVDC links (e.g. point-to-point) is a Multi-Terminal Direct-Current (MTDC) which deploys more than two HVDC station terminals, ultimately creating a DC grid. An MTDC grid can further advance the techno-economical offerings of HVDC technology and therefore accelerate the supergrid realization. However, the are still technical outstanding challenges to be resolved and hence it is not a trivial task to design and operate an MTDC supergrid. Consequently, it is of utmost importance to investigate, analyze and mitigate the emerging challenges introduced by MTDC systems in order to promote their widespread deployment.

To enable more efficient interchange of power and also to harness RES, there is a business case for setting up a European Supergrid. A supergrid can be defined as a transmission backbone which allows massive integration of RES [6]–[8]. It has the ability to connect different remote energy sources to an existing grid, offer improved controllability, bring efficient energy balance over a wide geographic spread, and most significantly, allow a more diversified energy portfolio. There are several concepts for the topological setup of such a supergrid, proposed by several organizations which are depicted in Figure 1.

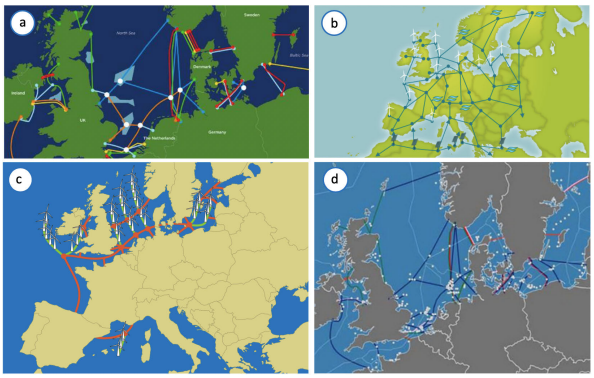

FIGURE 1. European Supergrid concepts: a) Wind Energy Europe [4], b) Friends of Supergrid [3], c) Airtricity [2], d) European Commission [5].

Besides the European Supergrid, there are proposed concepts for setting up supergrids in Asia and United States of America [1], which are shown in Figure 2a and Figure 2b respectively.

It is therefore evident that in many respects, the development of a wide HVDC-based supergrid is a well-crafted strategy, especially in Europe due to its leading role in RES. Even though HVDC technology introduces many major advantages (refer to Table 1) which future supergrids are based upon, it is also accompanied by several technical barriers and challenges.

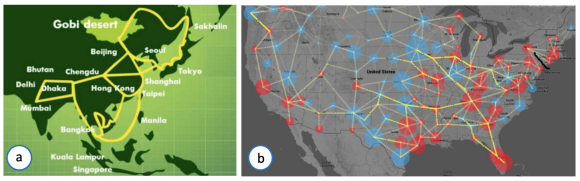

FIGURE 2. Non-European Supergrid concepts: a) North-East Asia [9], United States of America [8], [10].

TABLE 1. VSC HVDC trade-offs.

Advantages	Challenges
Interconnection of asynchronous AC grids	DC-side fault management
Transmission constraints mitigation	Equipment standardization
Flexible integration of RES	Grid code establishment
Improved market efficiency	Transnational cooperation
Fast power flow control	Complex control systems
Connection to weak AC grids	Development of pricing mechanisms
Enhancement of AC system stability	Generation of harmonics
Reduced pylon and cable profile	Compound grounding systems
Long-distance bulk power transfer	Low availability-reliability
Less visual impact	Environmental challenges

Despite the fact that there several issues to be resolved for the widespread deployment of MTDC grids, there are specific challenges associated with DC-side fault management, which is a very critical issue when considering HVDC technology. In order to capture DC-side fault transients for protection, control and fault location applications, measuring equipment is required to be placed on HVDC installations. This paper mainly focuses on reviewing the available technologies from the perspective of enabling protection, fault location and automation applications in HVDC systems. Even though some relevant review on protection and fault location functions has been conducted in [11]–[13], the work did not provide any profound insight with respect to the element of measuring technologies towards achieving the desired characteristics of those functions.

Section II includes a review of protection and fault location functions, which are sorted according to voltage and current measurements, communication and sampling frequency requirements. Sections III and IV provide a detailed analysis and discussion of the voltage and current sensing equipment for HVDC installations. Section V presents a mapping exercise of protection and fault location functions against the available voltage and current measuring technologies and essentially unlocks the insights for selecting measuring equipment. In Section VI this paper also analyzes and discusses the available options for automation applications, standards and protocols for HVDC installations in conjunction with the realization of the desirable measuring characteristics. Finally, conclusions are drawn in Section VII.

II. PROTECTION AND FAULT LOCATION IN HVDC GRIDS

For the practical operation and employment of MTDC grids, there are numerous technical outstanding issues to be solved. Major categories of these include power exchange control [14]–[16], dynamic behavior and stability [17]–[19], systems and grid integration [20]–[22] and finally, fault manage-

ment accounting for detection, protection and fault location [23]–[25]. Consequently, it is of utmost importance to investigate, analyze and mitigate the emerging challenges introduced by MTDC systems in order to promote their widespread deployment.

DC-side faults occurring in HVDC systems are generally characterized by large inrush currents (escalating over a very short period of time), initiated by the discharge of stored energy in the relevant capacitances of the entire system. Such capacitances can be found on the DC side of converters, transmission line capacitances, and also within modular multilevel converters (i.e. sub-module capacitors).

When DC-side faults occur in MTDC grids, the associated DC protection systems are anticipated to minimize the onerous effects by disconnecting the faulted sections while allowing the remaining healthy part of the grid to maintain its operational status. Such requirements imply the need for transient characterization of DC-side faults, ultimately leading to the development of reliable, fast, and sensitive DC protection methods. Therefore, one of the main objectives of protection area is to demonstrate solutions to mitigate the key challenges associated with the protection of MTDC grids, ultimately reducing the risk for the realization of HVDC-based supergrids.

Specifically, regarding fault-management issues in HVDC grids, according to 'ENTSO-E Code on HVDC Connections and DC-connected Park Modules' [26], HVDC systems (including overhead lines), shall have the capability to recover from DC-side transient faults. In addition to this, it is highlighted that with regard to priority ranking in the area of control and protection, the owner/operator of HVDC shall organize its control and protection equipment in order to comply with the following priorities, listed in decreasing order of importance:

- Protection (for HVDC and network systems)
- Control of active power (for emergency assistance)
- Synthetic inertia (if applicable)
- Automatic restoration actions
- Limited Frequency Sensitive Mode (LFSM)
- Frequency control and Frequency Sensitive Mode (FSM)
- Constraint of power gradient

It is therefore evident that protection is of the highest importance for the healthy operation of HVDC grids.

Additionally, as reported in 'IEEE Guide for Establishing Basic Requirements for High-Voltage Direct-Current Transmission Protection and Control Equipment' [27], along with the HVDC protection equipment, the following important subsystems should interact closely and effectively to implement the required functions:

- DC line fault locator
- Electrode line monitoring equipment
- Transient fault recorder
- Station clock synchronization equipment
- Harmonics monitoring equipment
- Converter valve cooling control and protection equipment
- DC measuring equipment

Therefore, fault location is another important function required to run alongside protection. This is due to the fact that after the successful detection and isolation of a fault, and assuming the fault is permanent, the meticulous estimation of its location is of significant importance as a means to accelerate the line restoration, reduce downtime of the system, limit recovery and repair costs, and hence elevate the overall availability and reliability of the transmission system. This is particularly important in the case of a supergrid, where a single unit disconnection can tremendously affect power exchange between different countries.

In Table 2 and 3, the design elements for a variety of DC protection and fault location solutions found in the technical literature have been summarized, showcasing among others the necessary sampling frequencies in each case. The required sampling frequency is practically enabled by appropriate measuring and sensing equipment. A detailed analysis of protection and fault location can be found in Appendix A and B respectively.

III. VOLTAGE MEASURING TECHNOLOGIES

A. RESISTIVE-CAPACITIVE VOLTAGE DIVIDER

In VSC-based HVDC systems, measurement of voltage is usually obtained using a resistive-capacitive (RC) voltage divider [6], as shown in Figure 3. The resistors connected in parallel to the capacitors are designed to guarantee an extremely low resistance variation through time, electrical stress and temperature [115]. Single- or double-shielded coaxial cables are used to transmit pulses from one end to another, preserving the information in the signal. To prevent any possible reflection phenomena (occurring mainly during fast transients), the coaxial cable is usually terminated with an external burden impedance. Resistive-capacitive voltage dividers are capable of generating an accurate voltage over a wide frequency band (typically from DC up to 500 kHz) [115], [116].

Considering the design depicted in Figure 3, the voltage V_2 obtained at the low-voltage side of the RC divider can be given by:

$$\frac{V_2}{V_{dc}} = \frac{R_2}{R_2 + R_1 \frac{1+R_2 j\omega C_2}{1+R_1 j\omega C_1}} = \frac{C_1}{C_1 + C_2 \frac{1+1/R_2 j\omega C_2}{1+1/R_1 j\omega C_1}} \quad (1)$$

Expression in equation (1) is valid considering that the following design criterion is met:

$$R_1 \cdot C_1 = R_2 \cdot C_2 \quad (2)$$

Pure capacitive or inductive voltage dividers are not well-suited for capturing fast transients due to their limited transfer behavior leading to narrow frequency bands as show, in Figure 4 [115], [117].

TABLE 2. Taxonomy of HVDC protection systems according to voltage, current, communication and sampling frequency requirements.

Method	Measurements		Communication requirement	Sampling frequency	Detection functions
	Voltage	Current			
[28]	×	✓	×	2 MHz	$\Delta i, TWFSR$
[29]	×	✓	✓	1 MHz	Δi,
[30]	✓	✓	×	1 MHz	$di/dt, DCWT(v)$
[31]	✓	×	×	500 kHz	$UV, DWT(v)$
[32]	✓	✓	×	200 kHz	FPT, UV
[33]	✓	✓	×	200 kHz	$UV, fit(i)$
[34]	✓	✓	×	200 kHz	$UV, fit(i)$
[35]	✓	✓	×	200 kHz	$fit(i), dv/dt$
[36]	✓	✓	×	110 kHz	$SATD$
[37]	✓	✓	×	100 kHz	$SWT, di/dt$
[38]	✓	✓	×	100 kHz	$UV, dv/dt$
[39]	×	✓	✓	10 & 100 kHz	$DWT(i), \Delta i, sgn(i)$
[40]	×	✓	✓	100 kHz	Δi
[41]	×	✓	×	96 kHz	$WE(i), WER(i), WTMM(i), sgn(WTMM)$
[42]	✓	✓	×	96 kHz	$CovoI, CWT(v), \Delta I$
[43]	✓	✓	×	50 kHz	$HHT, di/dt, UV$
[44]	✓	×	×	50 kHz	$d\bar{I}, \Delta i$, peak detection
[45]	✓	×	×	50 kHz	$ROTV$
[46]	×	✓	×	50 kHz	$DFT(i), THFE$
[47]	✓	✓	×	50 kHz	OC, v and i locus
[48]	✓	✓	×	50 kHz	$dv/dt, di/dt, \Delta v$
[49]	✓	×	×	50 kHz	QCD
[50]	×	✓	✓	50 kHz	$DiroI, DWT(i)$
[51]	✓	×	✓	50 kHz	$\nabla v, \int V_{Ldc}$
[52]	✓	✓	×	25 kHz	$di/dt, DWT(v)$
[53]	✓	×	×	25 kHz	
[54]	✓	✓	×	20 kHz	$FSC, UV, dv/dt, di/dt$
[55]	✓	✓	×	20 kHz	$WT, FFT, du/dt, \Delta i, \Delta v$
[56]	✓	×	×	20 kHz	$dv/dt, VCI, TVE$
[57]	✓	✓	×	20 kHz	$sgn(dv/dt), sgn(di/dt), d(i/v)/dt$
[58]	✓	✓	×	20 kHz	$\nabla v, SATD, dv/dt$
[59]	×	✓	×	20 kHz	$di/dt, \Delta i, sgn(i)$
[60]	✓	✓	✓	20 kHz	TER
[61]	✓	✓	×	10 kHz	$CRP, du/dt, di/dt, UV$
[62]	✓	✓	×	10 kHz	OC, UV
[63]	✓	✓	×	10 kHz	$DWT(u), DWT(i), ConvoP, CPTE$
[64]	×	✓	×	10 kHz	$MAD(v), MAD(i)$
[65]	✓	✓	×	10 kHz	$S-Transform$
[66]	✓	×	×	10 kHz	$RT-BWT(v)$
[67]	×	✓	×	10 kHz	$ROHTLFC$
[68]	×	✓	×	10 kHz	$TVAC$
[69]	✓	×	×	10 kHz	$HFTVE$
[70]	×	✓	×	10 kHz	$WPEE$
[71]	×	✓	×	10 kHz	ANN on high frequency currents
[72]	✓	✓	✓	10 kHz	$CSoTW$,
[24]	×	✓	×	>10 kHz	di/dt
[73]	✓	✓	✓	10 kHz	$UV, OV, di/dt$, Nave Bayes classifier
[74]	×	✓	×	10 kHz	$TVAC$
[75]	✓	✓	✓	10 kHz	$DVTW$
[76]	×	✓	×	5 kHz	$di/dt, \Delta i$
[77]	✓	✓	✓	5 kHz	CSD
[78]	×	✓	×	2 kHz	$OC, di/dt, WT, PCA, GFS$
[79]	✓	✓	✓	–	TWD
[80]	✓	×	×	–	dv/dt
[81]	✓	×	×	–	dv/dt
[82]	✓	×	×	–	$dv/dt, sgn(dv/dt), peak(dv/dt)$
[83]	×	✓	×	–	UV,OC
[84]	✓	✓	×	–	dv/dt,di/dt
[85]	✓	✓	×	–	$SWT, dv/dt, UV, WCoV$
[86]	×	✓	×	–	$UV, \Delta v$
[87]	✓	✓	×	–	$dv/dt, di/dt$
[88]	✓	✓	×	–	$UV, OC, sgn(i)$
[89]	✓	✓	×	–	$UV, dv/dt, di/dt$
[90]	×	✓	✓	–	Δi
[91]	×	✓	✓	–	$\Delta i, OC$
[92]	✓	✓	×	–	UV, OC, v and i locus
[93]	✓	×	×	–	$dv/dt, \int V_{Ldc}$
[94]	×	✓	×	–	$CLRP(i, di/dt)$

The features of RC dividers which make them a very compelling option for measurement of voltage are listed below [115], [116]:

- No saturable cores leading to ferroresonance-free characteristics
- Superior transient characteristics
- Compliance with secondary technology base on microprocessors
- Design enabling short-circuit proof characteristics
- No need for disconnection for commissioning purposes (e.g. cable test)
- Significant width and weight minimization

B. OPTICAL SENSORS BASED ON POCKELS EFFECT

An optical electric sensing technology utilizing the Pockels effect is presented in [118]–[122]. Such optical voltage sen-

TABLE 3. Taxonomy of HVDC fault location systems according to voltage, current and sampling frequency requirements.

Method	Measurement		Sampling	Detection
	Voltage	Current	frequency	function
[95]	×	✓	2 MHz	$CWT, ATTW$
[96]	✓	✓	2 MHz	$CWT, ATTW$
[97]	✓	×	1 MHz	$HHT, ATTW$
[98]	×	✓	1 MHz	$WT, ATTW, GTBL$
[99]	×	✓	1 MHz	$EEMD,HHT$
[100]	✓	✓	1 MHz	$ATTW$
[101]	✓	✓	1 MHz	$ModVel$
[102]	✓	×	1 MHz	$ATTW$
[103]	✓	✓	500 kHz	$EML, WT, S-Transform$
[33]	×	✓	200 kHz	GLF
[104]	✓	×	200 kHz	DWT, SVM
[25]	×	✓	135 kHz	$\Delta i, ATTW$
[105]	✓	✓	100 kHz	DNF
[106]	✓	×	100 kHz	$1D-CNN, HHT, EMD$
[107]	×	✓	96 kHz	$\rho(d,x), WAF$
[108]	✓	×	80 kHz	$SMVS, PCC$
[109]	✓	✓	50 kHz	FLC
[110]	✓	×	50 kHz	$VPI, ATTW$
[111]	✓	✓	6.4 kHz	$MVVDF$
[112]	×	✓	5 kHz	$PCC, CWT, \Delta i$
[113]	×	✓	5 kHz	$EMTR$
[114]	✓	✓	1-4 kHz	SVM

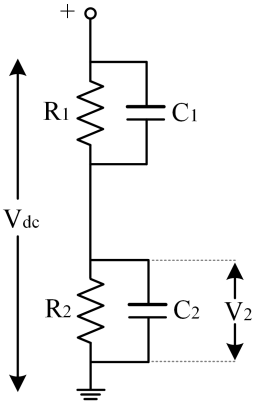

FIGURE 3. Resistive-capacitive voltage divider.

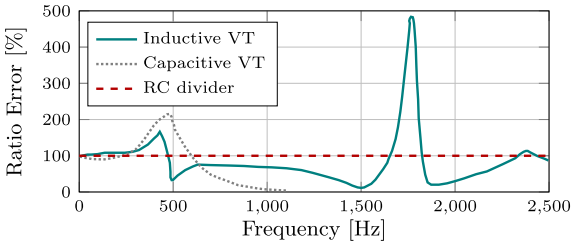

FIGURE 4. Comparison of bandwidth of an inductive VT, a capacitive VT and an RC divider [115].

sors are used in applications where wide frequency range is required and overcome some shortcomings of the conventional voltage sensors while using simpler structure and presenting better accuracy. Specifically, an optical sensing system is realized by combining the longitudinal Pockels effect and the optical technology as reported in [119]. The sensing scheme is used for measuring high-voltage levels up to 400 kV in a wide frequency range from DC to 30 MHz. In addition, [120] presents an improved optical HVDC measuring system using a Pockels crystal in a longitudinal modulation arrangement and two-wavelength laser systems in order to expand the measurable voltage range. The developed

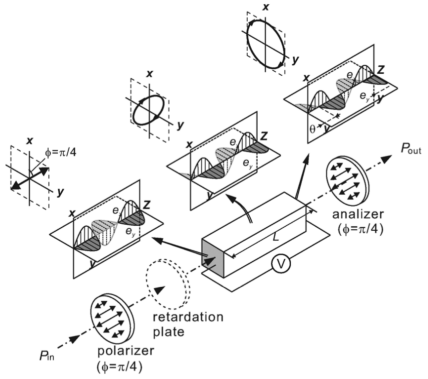

FIGURE 5. Voltage measurement based on the Pockels effect [120].

system is used for directly measuring high voltages up to 450 kV in the DC to GHz frequency range.

The electro-optic effect can be expressed by the change in the refractive index of the crystals under the effect of an applied electric field or voltage [120], [122]. Figure 5 shows an amplitude modulator in longitudinal modulation arrangement with a polarizer, oriented at 90^o with respect to an analyzer.

The linearly-polarized light propagates along the z-axis of the Pockels crystal, while the polarization status changes based on the Pockels effect of the crystal. Optical voltage sensors usually use BGO crystal. The induced phase retardation δ between two orthogonal optical components of the output light is given by [122]:

$$\delta \frac{\pi l}{\lambda} n_0^3 \gamma_{41} E = \frac{\pi V}{V_\pi} \tag{3}$$

where λ is the wavelength of the light, n_0 is the ordinary refractive index of the crystal, l is the length of the crystal, E is the exterior electric field, γ_{41} is the electro-optic permittivity, V is the measured voltage applied to the sensor and V_π is the half-wave voltage defined as the value of the V when δ reaches the π, and is given by [119]–[121]:

$$V_\pi = \frac{\lambda}{2 n_0^3 \gamma_{41}} \tag{4}$$

The output light intensity of the polarization beam splitter (PBS) analyzer is given by:

$$I_o = I_i sin^2 \left(\frac{\pi}{2} + \delta\right) = \frac{I_i}{2}\left(1 + sin(\frac{\pi V}{V_\pi})\right) \tag{5}$$

where I_i is the incident light intensity. When δ has a small value, $sin(\frac{\pi V}{V_\pi})$ can be replaced by $(\frac{\pi V}{V_\pi})$ and therefore (5) becomes

$$I_o = \frac{I_i}{2}(1 + \frac{\pi V}{V_\pi}) \tag{6}$$

Equation above indicates that the modulated light of the output intensity is a function of the measured voltage [122] and therefore, a voltage measuring device for HVDC installation can be realized.

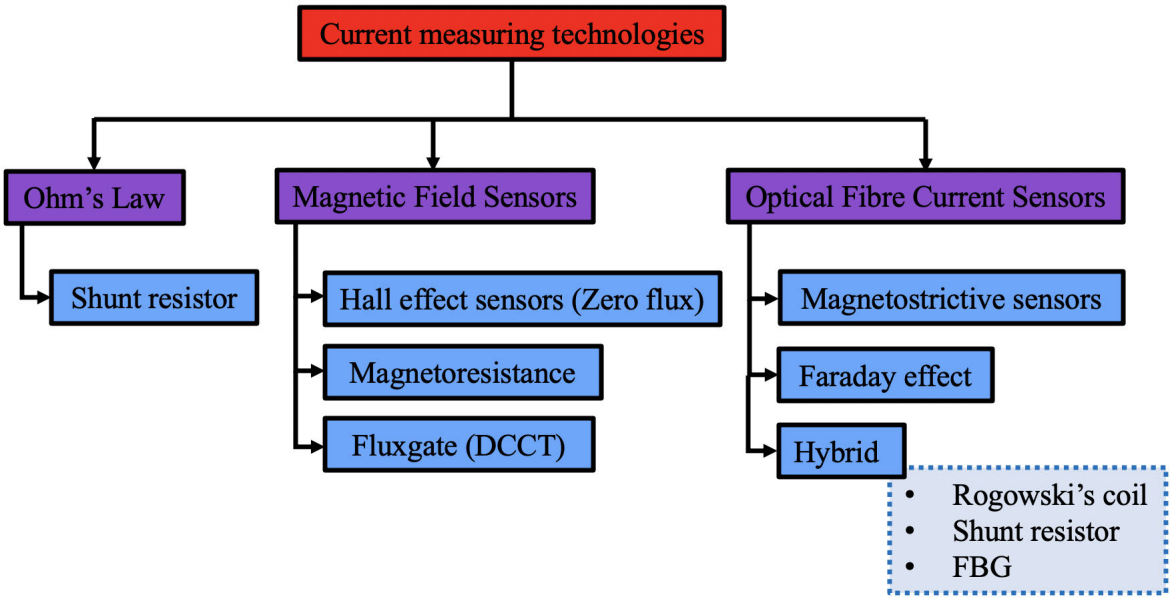

FIGURE 6. Classification of DC current measuring technologies.

However, the use of the aforementioned sensing technology for DC voltage measurements includes some uncertainties which are affected by several factors like the light source, the current-to-voltage converter and the unwanted cross electric field [119]. Furthermore, some technical challenges which have to be addressed include:

- The moving electric charges in the crystal causes drift of the output intensity of the light sources
- The modulated signal of the DC voltage is difficult to be distinguished from the light intensity

IV. CURRENT MEASURING TECHNOLOGIES

Reliability and accuracy of DC current measurement are significant requirements for HVDC control and protection purposes. Figure 6 illustrates the various current measuring technologies that are currently available and appropriate for HVDC applications. The rest of this section describes in detail the operation principles and characteristics of DC current sensors, while special emphasis is paid on their current measurement range, accuracy and bandwidth.

A. OHMS LAW - SHUNT RESISTOR

The well-known Ohm's law states that the current that flows through a resistor is directly analogous to the voltage drop across this component. This simple principle can be utilized to measure currents.

A simple means of current measurement is the use of a shunt resistor with low ohmic value that is directly connected into the main current conduction path. The voltage that is measured at the pins of the resistor represents a proportional measure of the current that flows in the circuit. Because of the direct integration into the main circuit, shunt resistor can generate substantial power losses and reduced efficiency, especially in high current applications (losses are proportional to the square of the measured current).

This sensing technology is relatively simple, reliable and is applicable for both AC and DC technologies with a measurement bandwidth up to several MHz [123]. A number of factors can affect accuracy performance, such as temperature effects, mechanical forces and thermoelectric voltages. From the several available implementations, the squirrel cage shunt that consists of parallel manganese and copper bars is suitable for high current applications due to its low thermoelectric voltage and temperature coefficient [124]. Moreover, the impedance of the shunt can increase as frequency increases due to the proximity and skin effect. [125], [126]. The frequency dependent characteristic of the shunt can be mitigated by suitable selection of the radius of the conductors and the distance between the conductors [127]. However, lack of galvanic isolation is the main disadvantage of shunt resistors.

B. FARADAYS LAW OF INDUCTION

Faraday's law of induction has been widely used for current sensors in AC applications. The greatest advantage of sensors based on Faraday's law, is that they provide isolation between the current to be measured and the output signal [128]. This property is very important in control and protection applications because existing safety standards demand electrical isolation. The current transformer and the Rogowski coil are the two most representative sensors that have been designed based on Faraday's law. Although these current sensing techniques are not suitable on their own for DC current measurement, their principles and characteristics are presented, since they are commonly used in hybrid DC current sensors that combine more than one technology (e.g. optical fiber sensor

with a Rogowski coil), or in devices with extra components that permit DC current measurements

The working principle of both sensors is explained through the Ampere's law that relates the magnetic flux density around a loop to the enclosed current that passes through the loop, as shown in equation (7)

$$\oint_C \vec{B} \cdot \vec{dl} = \mu_0 \mu_r i_c \tag{7}$$

When the primary current i_c flows in the center of the loop, the flux density B is given by

$$\vec{B} = \frac{\mu_0 \mu_r i_c}{2\pi r} \tag{8}$$

This relationship is used in conjunction with Faraday's law of induction for both sensors of this family to calculate the induced voltage in the measurement winding, which is proportional to the main current.

1) CURRENT TRANSFORMER

A typical construction of current transformer (CT) consists of a core material with high relative permeability and two windings. The main current flow path serves as the only primary turn, while several secondary turns are employed to provide a representative measurement of the main current. Similar to a conventional transformer, the primary current is translated to a secondary current with a magnitude that is dictated by the turns ratio of the windings. Thus, the secondary winding together with the core form the measuring head of the CT. A carefully designed resistor (R_s) is connected in the secondary winding. The magnetic flux generated by the secondary current that flows through R_s counters the flux generated by the main current. The purpose of this resistor is to convert the generated compensated current into a voltage signal. The induced voltage can be derived as follows

$$u = -N\frac{d\phi}{dt} = -NA\frac{dB}{dt} = -\frac{NA\mu_0\mu_r}{2\pi r}(i_c - Ni_s)\frac{d}{dt} \tag{9}$$

where i_c is the primary current, i_s the secondary current and μ_r the relative magnetic permeability of the core material. Solving this equation for i_s yields the following equation

$$i_s = \frac{i_c}{N} - \frac{l_m}{N^2 A \mu_0 \mu_r}\int_t u_s dt \tag{10}$$

The above equation implies that the current transformer is unable to measure DC currents and consequently, additional modifications are required to perform this task.

2) ROGOWSKI

Similar to the current transformer, the Rogowski coil or air-core coil current sensor exploits Faraday's law in order to measure currents. The main differences compared with the basic construction of a current transformer is that the Rogowski coil uses a non-magnetic core material and it does not include the burden resistor in the secondary winding. The measuring head consists of a coil that is wound uniformly around a non-magnetic former, which in turn forms a closed loop around the main current carrying conductor. The conductor's position needs to be in the center of the coil to mitigate measurement errors [128].

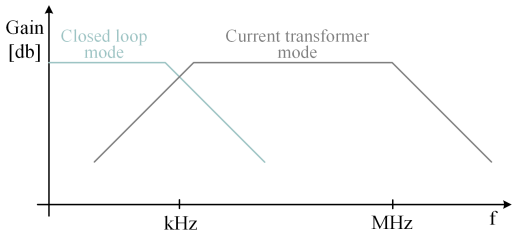

FIGURE 7. Typical illustration of bandwidth for closed-loop and CT mode.

According to Faraday's law, a voltage is induced in the Rogowski coil that is proportional to the rate of change of current as shown by:

$$u = -N\frac{d\phi}{dt} = -\frac{NA\mu_0}{2\pi r}\frac{di_c}{dt} \tag{11}$$

where N is the number of turns and A is the cross-sectional area of the former. This equation shows that the voltage is proportional to the derivative of the main current i_c that needs to be measured. Hence, an integrator is employed to produce a signal that is directly proportional to the main current. Since the main principle of this sensor relies on the detection of a change in flux (i.e., current change), Rogowski coil cannot be directly used to measure DC currents. Owing to the absence of a magnetic core, the Rogowski coil demonstrates very good linearity and is capable of carrying very large currents (tens of kAs) over an extended bandwidth up to several tens of MHz [129]. Recently, current sensors have been designed based on the Rogowski coil principle that can be fabricated using a printed-circuit board (PCB), appropriate for installation in individual modules of power converters, demonstrating high accuracy and extended bandwidth [130], [131].

C. MAGNETIC FIELD SENSORS

As analyzed in Section IV-B, current sensors based on Faraday's law of induction are not capable of sensing static magnetic fields. On the contrary, magnetic field sensors can recognize and respond to static magnetic fields. Moreover, CT and Rogowski coil perform remarkably well in the high frequencies region, while magnetic field sensors perform better for lower frequencies. Therefore, it seems sensible to combine either a Rogowski coil or a current transformer with magnetic field sensors in order to build a current sensor with an extended bandwidth from DC to several MHz. The resulting effect of such combination in terms of frequency range and gain, is illustrated in Figure 7.

There are three main categories of magnetic field sensors: i) Hall-effect sensors, ii) sensors based on the fluxgate principle and iii) magnetoresistors. All three of them can be used in an open-loop or in a closed-loop sensing configuration. In open-loop arrangements, the field sensor can be placed in the vicinity of the main current conductor

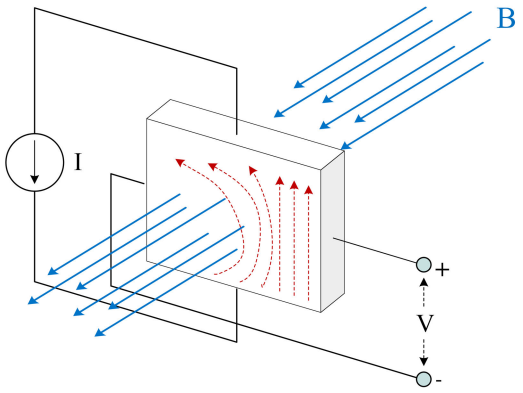

FIGURE 8. Illustration of Hall effect through a conductive material.

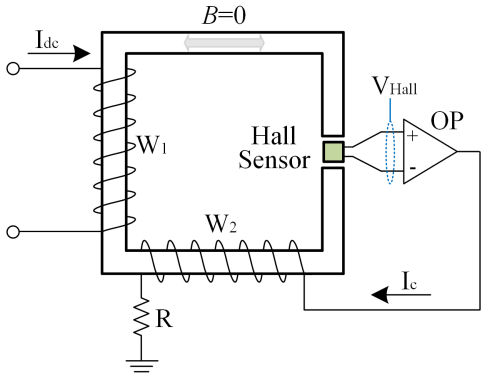

FIGURE 9. Zero flux DC current transformer.

or alternatively, a magnetic core is used to concentrate the magnetic field that is generated from the enclosed conductor onto the magnetic field sensor that is situated in the airgap of the core material. The former is susceptible to the skin effect and external magnetic fields, while in the latter configuration the sensitivity is substantially improved due to the high magnetic permeability of the core material, and the skin effect is eliminated. Nevertheless, excessive currents can lead to the saturation of the core, in which case degaussing is required. Additional limiting factors for both topologies are the relatively low bandwidth and the significant thermal drift of the sensing element [128]. Nevertheless, the open-loop configuration constitutes a simple and cost-effective solution.

In the closed-loop configuration, the magnetic field sensor's output voltage is used as a feedback control signal to drive a compensating current in a secondary winding. This is wound in the magnetic core to counter the magnetic flux that is generated by the primary current. This configuration results in a zero-flux transducer. With the use of a secondary winding, the transducer operates as a current transformer in the high frequency region, resulting in extended bandwidth [132]. The closed-loop sensing configuration reduces significantly or eliminates the thermal drift and dramatically improves the performance of the sensor [133]. Complexity and extra cost are the limitations of this technology.

1) HALL-EFFECT SENSOR

Hall effect-based sensor is the most widely-used magnetic field sensor. Its working principle is designed around the Hall effect that is illustrated in Figure 8.

The effect describes that when a current flows through a conductive material in the presence of a magnetic flux density that cuts through the surface of the conductor, a voltage is induced that is perpendicular to both the magnetic field and the current. The effect can be described mathematically as:

$$V = \frac{IB}{nqd} \tag{12}$$

where n is the charge carrier density, q is the charge of each electron, and d is the thickness of the conductive material. Although the Hall effect is very small in metallic conductors, the effect is enhanced when semi-conductors are used [134]. Indium arsenide (InAs), Gallium arsenide (GaAs) and Aluminium Gallium nitride or Gallium nitride AlGaN/GaN are typical materials used for the construction of Hall effect-based sensors [128], [135].

Hall effect-based sensors can be used in both open-loop and closed-loop configurations. Closed-loop transducers, which are also called Hall effect-compensated or zero flux current transformers are commonly used for the measurement of DC current in HVDC applications [6], [116]. A typical structure of the transformer can be seen in Figure 9 [136], which consists of two windings (W_1 primary and W_2 secondary), a magnetic core, a Hall effect-based sensor and an operational amplifier (OP).

When primary current I_{dc} flows through winding W_1, it generates a magnetic field B in the core which induces a voltage V_{Hall} at the sensor output. The sensor output voltage V_{Hall} is almost proportional to the magnetic field, which in turn is proportional to the measured current. The primary current I_{dc} is compensated with current I_c fed to W_2 which results in zero flux ($B = 0$) in the magnetic core. When the primary current contains a DC component, the current proportional to this is fed to the input of the OP. The resulting compensation current I_c is a true-to-scale copy of the primary current [137]. Depending on the way of construction of zero flux DC transformers, bandwidths of up to 10 kHz for 25 kA maximum currents and up to 500 kHz for 5 kA maximum currents can be obtained [117], [133]. An alternative configuration based on the combination of Hall effect-based sensor with a Rogowski coil that achieves a bandwidth of 75 MHz has been reported in [138].

2) FLUXGATE SENSORS

The working principle of fluxgate sensors is essentially based on the detection of change in the inductance of the sensing element [133]. In its simplest form, a fluxgate transducer can be built in a similar manner with a Hall effect-based current transducer (refer to Figure 10), where the Hall effect-sensor is replaced with a fluxgate element. The sensing element comprises of a coil that is wound around a thin magnetic

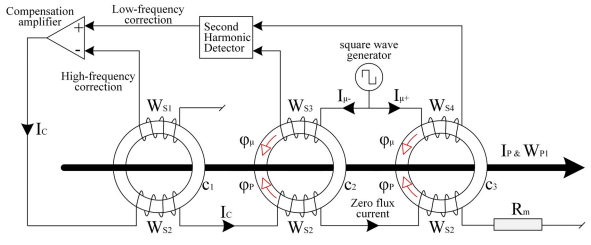

FIGURE 10. Closed-loop fluxgate transducer.

core. The underlying principle of this sensor depends on the detection of a change in the inductance of the coil.

The non-linear relationship between the magnetic field H and the flux density B for a magnetic material is utilized by the fluxgate technology. The value of the inductance of the sensing element is dependent on the magnetic permeability of the core. In detail, when the flux density is low, the inductance decreases, while when the flux density is high, the inductance increases.

The fluxgate element is designed in such a way that its saturation level varies with respect to the applied external field B_{ext}, produced by the primary current I_c, which provokes a change in the magnetic permeability of the core and hence, the inductance. Moreover, a current that is injected into the coil of the fluxgate element produces an additional magnetic field H_0 that also affects the inductance of the element. The frequency of the injected current can be increased to improve the sensor's accuracy [128]. The two magnetic fields may add or counter each other. Thus, the fluxgate transducer is developed in a way that near zero total flux corresponds to low inductance, and high flux leads to core saturation and therefore low inductance.

Various fluxgate transducers have been designed that use either open-loop or closed-loop configurations [139], [140]. In the closed-loop configuration, the variation of the inductance of the fluxgate element is measured and processed by adequately-designed electronics to manipulate the injected current with the aim to operate the core under zero flux conditions [141]. Subsequently, the measured current can be simply calculated based on the turns ratio. Figure 10 presents a closed-loop fluxgate transducer that has been manufactured by LEM [133]. In this configuration three magnetic cores are used with separate secondary windings, a common primary winding (current-carrying conductor) and a common compensation winding.

The closed-loop configuration is achieved with the injection of current I_s that flows in compensation windings. The transducer operates as a fluxgate sensor for low frequencies with W_{S3} and W_{S4} serving as the fluxgate elements, and as a current transformer in the high frequency region (W_{S1} and W_{S2}). The transducer achieves very high accuracy and extended bandwidth from DC to 100 kHz.

3) MAGNETORESISTORS

Magnetoresistors (MR) make use of the magneto-resistance effect, which describes the tendency of some materials, to vary the value of their resistance under the influence of an external field. MR sensors are developed based on metal alloys and present better sensitivity, measurement accuracy and higher bandwidth as opposed to Hall effect-based sensors [142]. This effect has been successfully used for the construction of read heads in magnetic recording but in the recent past, they have been examined for DC current measurement applications [134], [143]–[145]. Based on the magneto-resistance effect, several types of magnetic field sensors have been designed and three of the most appropriate ones for DC current measurement are subsequently described.

a: ANISOTROPIC MAGNETO-RESISTANCE (AMR) SENSORS

Within the family of MR sensors, AMR sensors are the most mature technology. The term anisotropic derives from the sensor's dependence on the angle between the direction of magnetization and the measured electrical current. The angle between the two affects the resistance of the ferromagnetic material and depends on the magnitude of the field. The resistance is at its maximum when the primary current flows in parallel with the magnetization and at its minimum when the current is perpendicular to the magnetization. AMR sensors are usually used in a Wheatstone bridge configuration and demonstrate a high frequency response up to 1 MHz, that is usually limited by the integrated necessary amplification stages to several hundreds of kHz [128], [146].

b: GIANT MAGNETO-RESISTANCE (GMR) SENSORS

GMR is another sensor that can also detect static magnetic fields. GMR effect is manifested in structures which comprise of thin magnetic layers separated by thin non-magnetic layers. Similar to the AMR effect, under the influence of an external magnetic field, the structure's resistance reduces significantly. GMR sensors can also be utilized in a Wheatstone bridge configuration and they are more sensitive than the AMR sensors [147]. The drawbacks of GMR technology include the relatively higher cost and lower bandwidth when compared to AMR technology [148].

c: TUNNELING MAGNETO-RESISTANCE (TMR) SENSORS

TMR sensors is a promising sensor technology that exhibits significantly higher sensitivity than current GMR and AMR sensors. A TMR sensor includes insulating layers rather than metallic layers that are employed by GMR sensors [148]. The sensor technology is at its early stages of development with limited applications. For high current applications, a prototype that is based on a combination of a TMR sensor with a Rogowski coil, has been proposed in [149].

D. OPTICAL CURRENT SENSORS

Optical current sensors for high voltage applications have received increased interest in the last decades, mainly because of their small size and weight, low power consumption and their capability to measure both DC and AC currents. Optical sensors are using optical fiber as the sensing element and hence, they provide inherent isolation and immunity against

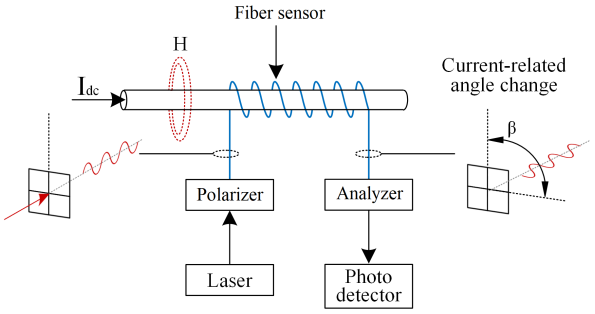

FIGURE 11. Optical fiber current sensor as per the Faraday effect.

electromagnetic interference, features that are of vital importance in high voltage applications. [150]. Current sensors based on optical sensing commonly rely on the Faraday effect (or magneto-optic effect).

1) OPTICAL SENSORS BASED ON FARADAY EFFECT

According to the Faraday effect, when left- and right-hand circularly polarized light waves pass through a transparent material under the effect of a magnetic field that is oriented in the same direction as the traversing light, the relative speed of the left- and right-hand circularly polarized light speed changes slightly causing a shift in the state of the resulting linearly polarized light. As such, the two light waves accumulate an optical phase difference in proportion to the field's strength. This optical phase difference β can be expressed by:

$$\beta = V \int \vec{H} \cdot \vec{ds} \tag{13}$$

where V is the Verdet constant that is dependent on the medium that is used for light transmission. The detection of a change in the state of polarization of light can be realized via the polarimetric and the interferometric detection schemes.

a: POLARIMETRIC DETECTION SCHEME

A typical scheme based on Faraday effect is the fiber polarimeter, depicted in Figure 11. In this scheme, a linearly polarized light wave is generated and then fed into a fiber coil with N turns that encloses the main current carrying conductor [150]. The light wave is then analyzed at the output of the sensor using a second polarizer and a photodetector.

The use of the fiber coil has the desirable effect of immunity to all other external magnetic fields apart from the magnetic field caused by the current inside the coil. The magnetic field H, is the result of current I_{dc} flowing in parallel with the fiber sensor. According to the Faraday effect, field H causes a rotation of the polarization plane by an angle β, that is expressed as:

$$\beta = VNI_c \tag{14}$$

Angle β represents a measure of the magnetic field inside the Faraday medium (fiber). The combination of the analyzer and the photo-detector converts and modulates the polarized light into an electrical signal, which in turns corresponds to the current to be measured. With respect to the light intensity I_0 of the source, the output light intensity is given by:

$$I_d = \frac{I_o}{2}(1 + sin2\beta) \tag{15}$$

Polarimetric devices experience severe linear birefringence effect that can distort the rotation of polarization, thus reducing the accuracy and sensitivity of the sensor [150]. To overcome such an issue, interferometric schemes have been developed as explained below:

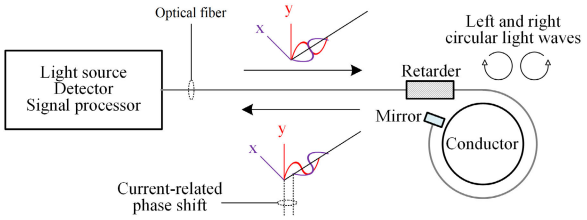

FIGURE 12. Reflective optical fiber current sensor.

b: INTERFEROMETRIC DETECTION SCHEME

In interferometric detection schemes, the linear polarization of light is analyzed into two orthogonal circular polarized light waves; a left-hand and a right-hand circular-polarized light wave. When the light waves pass through the fiber coil, the magnetic field that is created by the current to be measured slows the one component and accelerates the other, as a result of the Faraday effect. The shift between the two circular polarized light waves can be utilized as the detection signal.

A typical example of interferometric arrangement that exploits this effect is the Sagnac interferometer [151]. In this arrangement, the light from the source is initially polarized linearly and is split with the use of quarter wave retarders into two equal light beams with opposite circular polarization. The two-counter propagating light waves enter the fiber coil (Sagnac loop). After the two waves cross the Sagnac loop with different velocities, they are converted back to linear polarized light waves that now have a phase shift that is given by:

$$\phi_s = VN \int \vec{H} \cdot \vec{ds} = 2VNI_c \tag{16}$$

A phase modulator that generates a high frequency carrier is used to detect the optical signal, and the demodulation of the obtained signal retrieves the phase information. Open-loop Sagnac interferometer has been widely-used in HVDC applications [152]. The interferometer can also be used in a closed-loop configuration, where a control signal is fed back to the modulator to counter the current induced phase shift. In this case, the control signal is a direct measure of the phase shift and an image of the primary current [153].

In Figure 12 [154], a reflective fiber optic current sensor scheme is depicted which is an enhanced version of the Sagnac interferometer [151].

The presented scheme consists of an electronic device (light source, detector and signal processor), a retarder and a mirror. A simple optical fiber loop is wound around the conductor which carries the current to be measured.

As in Sagnac interferometer, the light source generates a light wave which is decomposed in left and right circularly polarized light waves which travel along the sensing fiber coil. The waves are then reflected by the mirror and their polarization direction is swapped. When a DC current is flowing though the conductor, a current-related phase shift is present to the reflected wave. In comparison to the previous arrangement, the total phase shift is now doubled:

$$\phi_s = 4VNI_c \tag{17}$$

In a similar manner with Sagnac interferometers, the phase shift Φ_s is detected and analyzed by the detector and signal processor. In this configuration, temperature sensitivities and mechanical disturbances that are typically present in the Sagnac interferometer are significantly mitigated.

The aforementioned fiber-optic current sensor is commercially available by ABB [155], and can measure up to 500 kA DC currents with a $\pm 0.1\%$ accuracy. Similar performance has been achieved for the optical current sensors developed by NxtPhase (now Alstom) [156], and GE [157], [158].

Current interrogation techniques limit the available bandwidth of existing optical current sensors, mainly because of the requirements of the applications that they have been designed to be used. Typically, the output of optical current sensors is digital and is converted to other forms via a merging unit [159]. The sampling rate of the merging unit limits the available bandwidth of the optical current sensor [160]. However, the technology offers a high potential for a wide frequency range from DC up to several MHz. In [161], a methodology for several output interfaces has been proposed. The proposed system can use an output interface suitable for demanding high-bandwidth applications, such as fault transients in HVDC systems, that works separately from an output interface that is designed to be in line with existing national and international standards that typically require low bandwidth.

2) MAGNETOSTRICTIVE SENSORS

Magnetic field sensors exploit the magnetostrictive effect, according to which, a mechanical strain is induced in a ferromagnetic material when it is submitted to a magnetic field [150]. The magnetic material expands in the case of positive magnetostriction, and shrinks in the case of negative magnetostriction in the direction of magnetization. Magnetic field sensor applications typically include an optical fiber wrapped around a magnetostrictive material or the use of a Fiber Bragg Grating (FBG) with magnetostrictive coatings. Sensors based on FBGs allow for optical multiplexing and long-distance interrogation [150].

The mechanical strain can be measured with a FBG, that operates as a filter and is placed in the core of an optical fiber. FBGs can reflect light that lies in a certain wavelength range and leave the rest wavelengths unaffected. When the fiber is strained due to the magnetostrictive effect, the reflected wavelength changes. This change can be detected and analyzed as a function of strain that denotes the strength of the magnetic field.

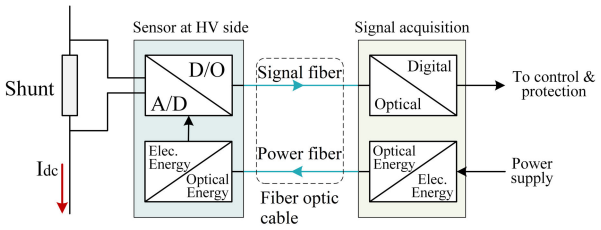

FIGURE 13. Layout of hybrid optical sensor scheme.

FBGs attached to magnetostrictive rods [162] or as a means of interrogating the displacement of the ferromagnetic material [163] have led to prototypes that allow DC current measurement for high power applications. Although magnetic field sensors present a promising solution, such sensors are not commercially available.

E. HYBRID OPTICAL CURRENT SENSORS

Hybrid optical current sensors combine standard current transducers such as Rogowski coil or shunt resistor, with optical fiber sensors. The conventional current transducer serves as the sensing element of hybrid devices, while the optical fiber system is used as the interrogation and transmitting element. The major advantage of hybrid sensors is that the fiber optic system provides galvanic isolation between the sensor head that measures the current in the main circuit at a high voltage level and the control system where these measurements are used. In this way, safe operation is ensured, insulation costs are significantly reduced, and the sensor is shielded from electromagnetic interference. The configuration of a hybrid optical sensor that is used for HVDC applications is shown in Figure 13 [124].

This sensor uses a direct shunt to measure the DC current that is located at high voltage together with an analog/digital voltage processing unit that converts analog measurements to optical signals. Then, an optical fiber data link is used for the transmission of the optical signals to the control/protection system that is located at ground level. This system contains a power supply and an optical processing unit that is used for the interrogation of the sensing element. In critical applications (e.g. for purposes of protection) redundant equipment can be used to enhance the reliability of the sensor. An additional Rogowski coil can be used in conjunction with the shunt resistor, where the latter is used for measurement of currents close to DC and the former is used to increase the overall bandwidth of the device [164].

In [25], [76], the authors presented hybrid optical voltage and current sensors which were demonstrated to be effective for both protection and fault location applications. In the studies presented, four FBGs inscribed in polyimide coated fibers, having a length of 7 mm, a bandwidth of 0.3 nm and peak

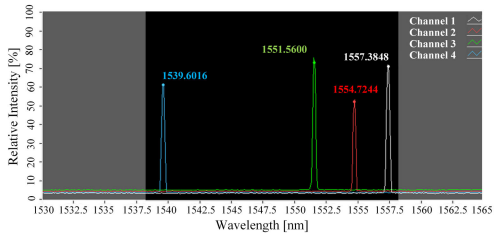

FIGURE 14. FBGs spectra [76].

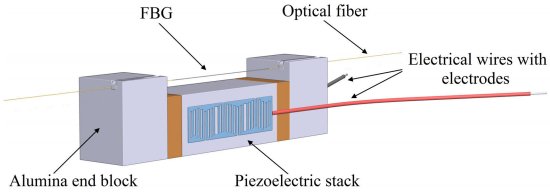

FIGURE 15. Hybrid FBG-based voltage sensor.

wavelengths at 1539.60, 1551.56, 1554.72 and 1557.38 nm (refer to Figure 14) were deployed to build four hybrid low-voltage sensors in order to prove the principle of the proposed protection and fault location schemes.

To construct a hybrid low voltage sensor, a 9 mm low voltage stack, having a maximum AC operating voltage of 30 V_{pk} (21.21 V_{rms}) was fixed between two alumina end blocks and a FBG sensor was pre-tensioned and epoxied to the ceramic blocks

For the construction of a hybrid (low-voltage) sensor, a voltage stack (P-883.11 PICMA from Physik Instrumente Ltd [165] was used) was placed between two alumina-based blocks. A FBG sensor (pre-tensioned) was epoxied (by utilizing EPO-TEK® 353ND) to ceramic blocks. The sensor structure is depicted in Figure 15. Considering that there is no mechanical forces in the piezoelectric part, the relative elongation $\Delta l/l$ introduced by an external electric field is given by:

$$\epsilon = d_{33}E = d_{33}\frac{V}{l} \tag{18}$$

where d_{33} is the longitudinal piezoelectric charge constant, E is the electric field, l is the length of the material and V is the voltage applied across the piezoelectric material [166].

Any voltage across the stack will produce a strain which is applied on the FBG, leading to a relative shift in its peak wavelength. Therefore, the shift on the peak wavelength can be calibrated in relation to the voltage [166].

Using this approach, an AC current measurement can be obtained by relating it with the FBG wavelength relative shift [167]. Effectively, a DC current sensor can be realized by utilizing a magnetostrictive transducer (instead of a piezoelectric component) [168]. Relative insulators could be used to cater for driving the fiber between the pole (which should be at ground potential) and the sensors placed directly on the current-carrying conductor. The optical fiber itself could be placed alongside the transmission line (e.g. within a trench)

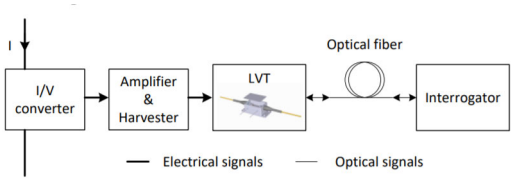

FIGURE 16. Optical current sensor for distributed measurements on HVDC networks [169].

or integrated within the cable or wrapped around the current-carrying conductor (very common practice in AC systems).

In [169], the authors proposed an optical current sensor for distributed current measurements on HVDC networks. The concept of the sensor is shown in Figure 16. A shunt resistor was utilized to convert DC line current into voltage. Voltage across the shunt resistor was amplified by a low power precision amplifier to drive an optical voltage sensor (LVT) combining photonic and piezoelectric technologies described above. The amplifier was powered from an energy harvester connected to the shunt resistor. Thus, no additional power supply provision was required for the amplifier at the sensor location. The prototype sensor was evaluated through laboratory testing and its performance was assessed within the context of the accuracy requirements specified by the relevant industry standards. It was demonstrated that the device has the potential to meet the requirements of the accuracy class 1 specified by the IEC 61869-14 standard.

The sensing schemes in [25], [76], [169] were experimentally tested at 5 kHz but greater sampling rates could be achieved if other type of interrogators were employed, e.g. a solid-state interrogator utilizing an Arrayed Waveguide Grating (AWG) as reported in [170]. In this case, the restricting factor for high-speed acquisition would be the performance of the utilized signal processing electronics, but frequencies higher than 100 kHz can be realized and the accuracy of relevant protection and fault location schemes could be improved significantly.

This technology has been found to be extremely beneficial for non-homogeneous feeders including both overhead lines and cables. In particular, as depicted in Figure 17 physical connection between cables and overhead lines, is realized at 'transition joint pits', and the connection of the actual current-carrying conductor is settled with 'transition joints'. Considering such a topological configuration, optical sensors can be installed throughout the transition joint and therefore DC current measurements can be achieved at transmission junctions.

V. MAPPING FAULT DETECTION & FAULT LOCATION FUNCTIONS AGAINST SAMPLING FREQUENCY AND MEASURING TECHNOLOGIES

In Tables 2 and 3 of Section II, the design elements for a variety of DC protection solutions have been summarized, showcasing among others the sampling frequency requirements. The proper function and performance of such DC fault detection and location techniques is greatly dependent on

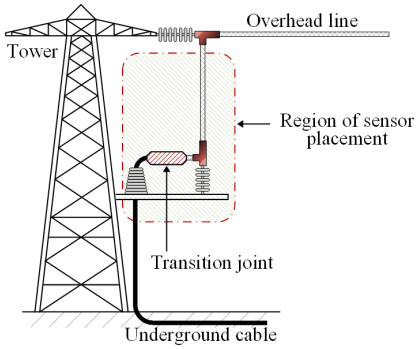

FIGURE 17. Typical outline of a transition joint pit [25].

the quality of measurements fed to the protection and fault location devices by the corresponding measuring schemes. This calls for an appraisal of the capabilities of existing voltage and currents measuring devices in terms of bandwidth requirements for the state-of-the-art DC fault location and detection functions.

With respect to voltage measurements, there is a limited number of options (refer to Section III). These mainly comprise of the RC voltage divider that achieves a high bandwidth in the order of MHz, and the hybrid optical voltage sensor that may emerge in future applications. The superior frequency response of the former, combined with its relative maturity, have rendered RC-voltage divider the main technology used in HVDC applications. By inspecting the frequency requirements of the various voltage-based DC fault detection and location functions, it is observed that they fall within the available bandwidth of RC-voltage divider. Hence, it can be concluded that voltage measurements for HVDC applications are considered readily accessible, indicating a competitive advantage of protection and fault location solutions that are based exclusively on voltage signals.

For current measurements, there is wider range of options, with each technology occupying a different frequency spectrum. In Figure 18, the current-based fault detection and location functions are mapped on a frequency diagram against the available current measuring techniques to illustrate the potential for applicability based on the existing technologies. It is worth noting that the frequency range achieved by each current sensing scheme, mainly refers to the bandwidth of the primary sensor, whereas the overall bandwidth of the complete measuring system may be further restricted by the secondary converter, the corresponding data acquisition system and signal-processing electronics.

An initial analysis of the diagram reveals a distinctive difference in the frequency range between DC fault detection and DC fault location functions. It is evident that the majority of DC fault detection solutions is concentrated in a frequency spectrum ranging from a few kHz to 100 kHz. This is explained by the fact that DC fault detection aims to detect every probable fault within the relay's protection zone, without the need for extremely accurate capture of fast transients during DC faults and therefore, high sampling frequencies are not typically required. This is especially true for unit protection schemes, which very often rely on simplified means of comparison between current measurements from both ends of the protected transmission medium. On the contrary, the vast majority of fault location functions utilizes sampling frequencies in the range of 100 kHz to 2 MHz. This is attributed to the fact that enhanced accuracy in fault location estimation is of paramount importance to expedite post-fault maintenance and reduce the downtime of the faulted component (e.g. DC cable). Hence, fault location methods require finer capture of fault transients, resulting in the utilization of significantly higher sampling frequencies.

Based on these findings, it is evident that there is greater variety of options among current measuring technologies for supporting current-based DC fault detection functions. In this case, the selection of the appropriate measuring instrument can be realized according to the sensor's reliability, accuracy, longevity, dynamic range, size and weight concerns, cost etc., while it is likely that there might be multiple current sensors that satisfy the required performance criteria. In the case of fault location functions with increased sampling rates, it can be seen from the diagram that the available sensors with the capability to measure faster fault transients are significantly reduced. It is noteworthy that group ⑫ approaches the bandwidth capacity limit of existing current instruments. Moreover, applications with high sampling rates are also accompanied with increased requirements in terms of signal processing electronics and advanced output interfaces, noise resilience, reliability and inevitably cost. Therefore, the implementation of such high-bandwidth demanding applications with suitable current instruments is a more complex task.

Taking Wavelet Transform (WT) and its variants (i.e. DWT, CWT, SWT) as an example, it can be noticed from the diagram that they are used as the main function in several DC fault detection algorithms (groups ①-⑧), in which sampling frequencies are in most cases less or equal than 100 kHz. In addition, the same functions have been employed in several occasions for fault location purposes (groups ② ⑪, ⑫ and ⑰), in which the vast majority utilizes significantly higher sampling rates. Since DC protection and DC fault location are anticipated to be integral parts of future HVDC grids and given that voltage and/or current measurements are required in both cases, it is reasonable to assume that the measuring instruments will be shared for the purposes of both applications. Therefore, a convergence between the requirements of both applications is desired, especially in terms of sampling frequency. Based on the diagram, such a convergence seems to be achieved for sampling frequencies around 100 kHz that concentrate a significant proportion of the detection and location functions.

VI. INDUSTRY STANDARDS

A. IEC 61869

Voltage and current sensors are key components for realizing high-fidelity measuring voltage and current measurements.

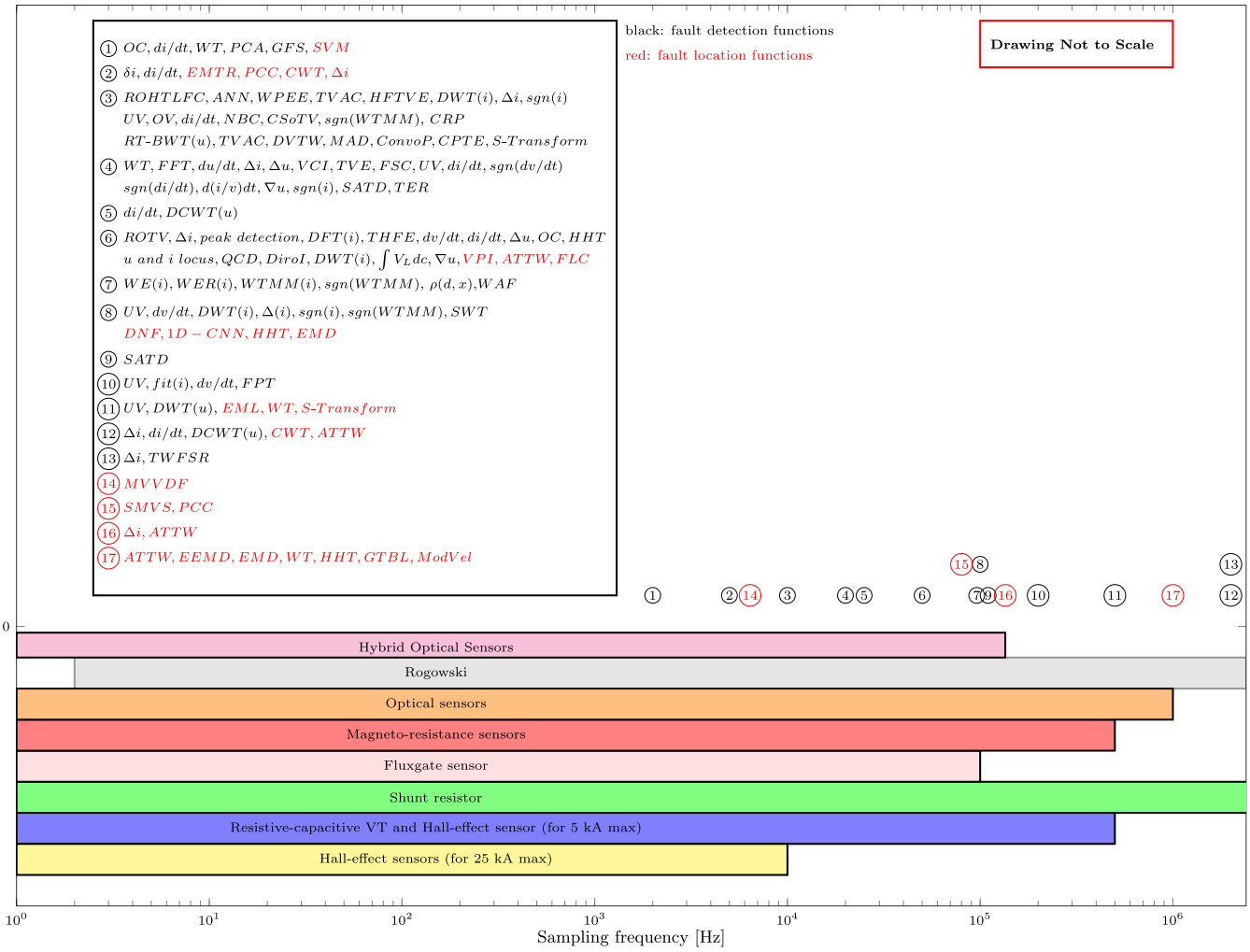

FIGURE 18. Mapping of fault detection and fault location functions against sampling frequency and measuring technologies.

With respect to measurements at HVDC installations the relevant industry standard for the instrument transformers is the International Standard series IEC 61869. It covers the needs and the requirements for the instrument transformers such as inductive current/voltage transformers low-power passive current/voltage transformers with analog output, electronic current/voltage transformers (with or without digital output) and current/voltage transformers for DC applications. Specifically, the IEC 61869-1 contains the general requirements and is valid for all instrument transformers [171]. IEC 61869-6 covers the specific requirements for the low-power instrument transformers used in a variety of applications including medium, higher voltages and DC applications. This part of IEC 61869 series defines the errors in case of the digital or analog output; includes metrological specifications regarding the class accuracy and detailed requirements for the frequency response [172]. Additionally, IEC 61869-14 and IEC 61869-15 cover instrument transformers used specifically in DC applications [173]–[176].

The general block diagram of single-phase instrument transformer is given in the Figure 19, and explains the

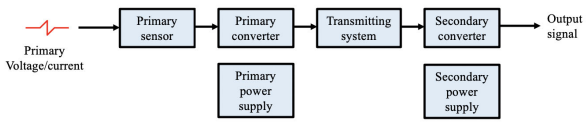

FIGURE 19. General block diagram of a single-phase LPIT [172].

measuring chain. Additionally, the possible configurations of instrument transformers are demonstrated in Figure 20 and are defined by the existing standard IEC 61869-6, released in 2016. The primary sensor and converter refers to a set of systems, which converts the primary current or voltage to an appropriate signal to be used by the transmitting system in order to be sent to the secondary converter, which provides the output signal for further processing.

Based on the configurations illustrated in Figure 20, it can be seen that there are four possible configurations for instrument transformers and the selection is subject to the specific application. Essentially, the only difference among the configurations depicted in Figure 20seems to be the existence

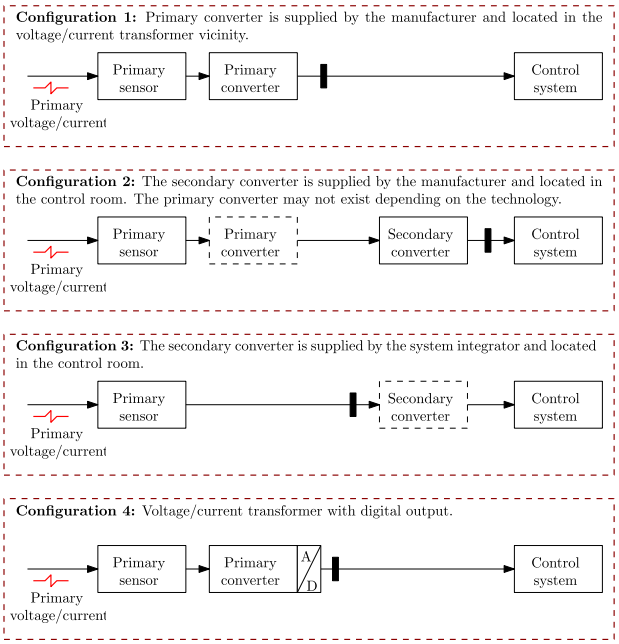

FIGURE 20. General block diagrams of possible configurations of voltage and current transformer for DC applications [173], [174].

of electronics with instrument transformers in form of either primary or secondary converter. The transmission link which can be either electronic (copper wires and Modbus protocol) or optical link to transmit the measurement data to relays or control rooms. This would also include electronic transformers with digital output covered by IEC 60044-7 [177] (replaced by IEC 61869).

For example, configuration 1 in Figure 20 is compliant with IEC 61869-10 and IEC 61869-11, which covers the additional requirements for low-power passive current (LPCTs) and voltage transformers (LPVTs), respectively. They are applicable to low-power passive instrument transformers with analog output, used for electrical measurements or electrical protection devices of the power systems [178], [179]. Configurations 2 and 3 could be used in applications, where signals should be further processed or converted prior to any processing by IEDs, merging units, etc. Configuration 4, for example, would be more applicable for sensors connected to merging units (where again analogue signals are converted to digital signals and transmitted to merging units using Sampled Values and GOOSE messages.

IEC 61869-10, released in 2017, covers the low-power passive current transformers with magnetic core or core-less like Rogowski coil, installed around the primary conductor. Their output can be either proportional to the primary current, or to the derivative of the primary current [178]. Passive current transformers do not include any active electronic components, which means that they do not use active primary converter (IEC 61869-8 refers to the electronic current transformers with active electronics). As per the Configuration 1 depicted in Figure 20, the primary power supply, secondary converter and the secondary power supply are not considered. In the case of the derivative LPCT, the air-core coil (Rogowski coil) is used as primary sensor and a transmission system is considered as well, while the primary converter is omitted. However, in the case of the proportional LPCT, the primary sensor corresponds to a ferromagnetic-core coil, and as primary converter a burden resistance connected to the coil output can be used. Specifically, proportional LPCT is composed of an inductive current transformer with primary winding, small core and secondary winding connected directly to a shunt resistor. Within this configuration a transmission system is utilized as well.

IEC 61869-11 covers the needs and requirements of the LPVTs without active electronics, which depend on the voltage divider principle. The voltage measurements are based on two working principles namely resistive and capacitive dividers. The output voltage of the voltage divider is substantially proportional to the primary voltage. The general block diagram of the single phase LPVTS corresponds to Configuration 1 in Figure 20, as it includes the primary voltage sensor, the passive primary converter and the transmitting cable. The secondary converter and power supplies are neglected, similarly to the LPCT configuration.

The requirements of the newly-manufactured instrument transformers anticipated to be used in DC applications, for voltages above 1.5 kV, are covered by the IEC 61869-14 and IEC-61869-15, in conjunction with IEC 61869-6 and IEC 61869-1 [171]–[176].

IEC 61869-14 and IEC 61869-15 are applicable to the current and voltage transformers for DC applications respectively (i.e. DCCTs and DCVTs) [173]–[176]. Such instrument transformers are composed by the primary sensors (with optional primary electronics), the transmitting system and the merging unit (refer to Configuration 4 in Figure 20). The primary converter is used to convert the primary, high amplitude signal to lower amplitude signal, which can be analog or digital, providing the input signal for the merging unit. This signal can be then converted to analog or digital format by the merging unit and it is sent to be further processed by the corresponding IED.

For voltage measurements, the primary sensor are resistive voltage dividers and mainly the RC dividers which can achieve the highest bandwidth (i.e. in the order of MHz). The primary element includes capacitive elements connected in series, and parallel to several resistors, which form the RC units. The secondary part includes the same type of elements (i.e. capacitors and resistors) connected in parallel but with different values in order to achieve the desired voltage ratio. It shall be noted that hybrid optical voltage sensors are expected to be used in the future DC applications [174], [176].

With specific reference to DC protection and fault location applications, the IEC 61869-9 promotes the sampling frequency of 96 kHz. However, the research investigating its performance and suitability is limited and has been reported in [41], [42], [180]. Within these studies it has been reported that a sampling frequency of 96 kHz is adequate for capturing DC-side fault transients and therefore can be utilized for protection purposes.

B. FURTHER RELEVANT STANDARDS

Recently, the HVDC digital substation concept is gaining attention, which is inspired by the approach followed in AC digital substations using the IEC 61850 standard series. In HVDC digital substations, current and voltage sensors are interfaced with merging units, which are responsible for converting and transmitting the measured voltage and current values to the various protection and control devices. IEC 61850-9-1 [181] and IEC 61850-9-2 [182] specify that sampled values (voltage and/or current measurements) are transmitted by the merging unit to the corresponding IEDs (through an intermediary process bus) at a rate of 80 samples per cycle for protection applications.

It is likely that a standard that will be an adaptation of IEC 61850 [183] may emerge for HVDC substations. Nevertheless, the communication rate of sampled values should be adjusted to satisfy the critical requirement for increased protection speed in HVDC grids, and to ensure agreement with the proposed sampling frequency by IEC 61869. For communication of teleprotection signals between different HVDC substations, the guidelines provided by IEC 60834 [184] on teleprotection equipment of power systems can be followed.

Best practices for improved reliability of critical substation functions would require duplication of certain equipment, such as Ethernet switches, and the use of communications protocols which manage redundant data streams. Guidance is given in IEC 62439-3:2020 [185]. Furthermore, provisions for digital substation cybersecurity are given in the IEC 62351 [186] series of standards.

A new edition of an IEC Technical Report (TR), IEC TR 61850-90-14 Edition 1 [187], is presently being drafted to guide the use of the IEC 61850 standards for HVDC technologies and Flexible AC Transmission Systems (FACTS) devices. This includes the use of IEC 61850 communications and data models for implementing control and protection systems for FACTS and HVDC, such as power oscillation damping control and fast-acting protective devices.

C. IMPACT OF COMMUNICATIONS SYSTEMS

1) OVERVIEW

HVDC protection and control applications may require input signals from multiple distributed measurement locations. FBG-based measurement methods can multiplex multiple voltage and current measurements on a single fiber to a central protection and control device [76]. Other sensor types typically require a communications network to transfer digitized measurement data, which could result in time delays and other undesirable impacts. Furthermore, the impact of communications on HVDC operation will depend on specific protection and control requirements, approaches, and algorithms. However, this section provides a general-purpose review of this impact.

The digitalization of measurements is increasingly being implemented in AC substations for increased efficiency, increased real-time performance, and reduced through-life costs, and this approach could also be applied in DC substations. However, as noted in Section VI-A, DC monitoring systems may require relatively high sampling rates to capture all relevant electrical transient phenomena, compared with typical AC system requirements. A sampling rate of 96 kHz, as defined in IEC 61869-9, is suitable for many DC applications, with the exception of detailed fault location, as identified in Section V.

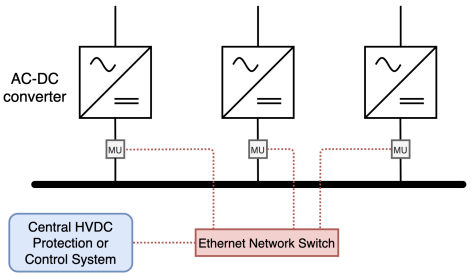

FIGURE 21. Generic representation of HVDC digital substation communications.

2) EXAMPLE APPLICATION

Figure 21 illustrates a generic HVDC digital substation, with three DC feeders. Each feeder has a Merging Unit (MU) to digitize voltage and current measurements, and potentially to control a local circuit breaker based on a coordinated command from a central protection or control system. An Ethernet network is used to transfer digitized measurements between devices. Note that it is possible for the MU to be integrated directly within the AC-DC converter, which would enable additional real-time protection and control functionality by communicating with the local power electronic converter control system.

Work conducted in [42] presents a method for calculating the maximum intrinsic measurement and communications delay, although excluding additional processing required by the sending and receiving devices, algorithm processing time, and time synchronization error. Based on the analysis in [37], the minimum delay for transfer of digitized measurement from the MU to the central controller is 36.06 μs (assuming a maximum of three ''competing'' simultaneous packets). Similarly, the minimum delay for a control command from the central controller to a MU, assuming a similar message size, is at least 25.64 μs (36.06 μs minus the 96 kHz sampling time of 10.42 μs), resulting in a total end-to-end communications delay of 61.7 μs. Note that this excludes the execution time for application-specific control or protection processing, and will vary based on the performance of the controller platform. Each additional MU would add at least approximately 10.78 μs (0.7 μs for a single Ethernet link transmission, 0.58 μs for additional switch queuing, and 9.5 μs for decoding the Ethernet frame), as they must be received serially by the central controller via its Ethernet connection; all other aspects contributing to the delay should occur in parallel with the other MUs.

VII. CONCLUSION

This paper outlined a detailed review of the available measuring technologies from the perspective of enabling protection, fault location and automation applications in HVDC systems. The review included the design elements for a variety of DC protection and fault location solutions, showcasing among others the sampling frequency requirements. The review ultimately revealed meaningful insights for selecting measuring equipment in conjunction with the desirable characteristics of protection and fault location systems. The performance of DC fault detection and location techniques is greatly dependent on the quality of measurements fed to the corresponding protection and fault location devices. The reviewed functions enabling protection and fault location of HVDC feeders, have been mapped on a frequency diagram against the available measuring techniques and devices, to illustrate the potential for applicability based on the existing technologies. It is worth noting that the frequency characteristics of each sensing scheme, primarily refers to the bandwidth of the primary sensor, whereas the overall bandwidth of the complete measuring scheme may be further restricted by the secondary converter and the corresponding data acquisition system and signal processing electronics. The review also identified that the use of RC voltage dividers has prevailed for voltage measurements for HVDC applications, due to their superior advantages. The choice of a suitable device for current measurement, depends mainly on the fault detection method used and the frequency range it operates. In particular, the review revealed that fault detection and protection methods are mainly concentrated in a frequency spectrum ranging from a few kHz to 100 kHz, while fault location methods require measurements with a frequency range starting from 100 kHz reaching up to 2 MHz. Since protection and fault location are expected to be integral parts of future HVDC grids, and given that voltage and/or current measurements are required in both cases, it is reasonable to assume that the measuring instruments will be shared for the purposes of both applications. Therefore, a convergence between the requirements of both applications is desired, especially in terms of sampling frequency. Based on the relevant analysis, such a convergence seems to be achieved for sampling frequencies around 100 kHz that concentrate a significant proportion of the detection and location functions. In particular, the sampling frequency of 96 kHz (as recommended by the IEC 61869-9 standard), can be satisfactory for both protection and fault applications, and therefore, a common measuring device could be used to comply with this standard.

APPENDIX A
DETAILED REVIEW ON PROTECTION METHODS
NON-UNIT PROTECTION SCHEMES

In HVDC non-unit protection methods, there is a notable trend towards the use of the inductive termination of DC transmission media to define protection boundaries. The deliberate inclusion of an additional series inductance not only restrains the rate of change of DC current but also influences the resulting DC voltage signatures. The fact that DC voltage during DC faults is different depending on fault location and the value of the inserted inductance at line ends (which is known in advance), can be exploited to achieve discriminative non-unit protection [38], [45], [53], [80]–[82], [86].

In [38], a two-stage approach is followed, in which fault detection is performed using an under-voltage criterion, and selectivity is ensured using a rate of change of voltage criterion. However, the proposed protection has not been validated for highly-resistive faults and only resistances up to 10 Ω have been investigated for pole-to-ground (PTG) faults.

In [80], DC voltage measurements from the line side of the inductor are utilized to obtain the rate of change of voltage and quickly detect and localize DC faults. Nevertheless, the converter DC voltage is assumed to remain unaffected immediately after the fault (which is not always the case), while resistive faults are not considered, which are likely to affect the performance operation of the protection method.

Both methods reported in [38] and [80] do not consider the impact of the transmission medium (e.g. differences between cables and overhead lines) and power reversal. Such studies have been carried out in [81], where a different approach is proposed using the rate of change of the DC voltage across the series inductor. However, the performance of the method for PTG faults has not been demonstrated.

The proposed algorithm in [24] calculates the ratios between the maximum rates of change of band-limited current measurements of different conductor pairs to indicate the type of fault. Based on the calculated ratios, five indices are defined to assist DC fault discrimination.

The method proposed in [28] uses current measurements sampled at 1 MHz to capture the first incident Travelling Wave(TW). The polarity of the current travelling wave is used to determine the fault direction and subsequently, the frequency spectrum ratio (FSR) of the current travelling wave is calculated. This ratio is directly proportional to the fault distance and hence, the fault zone and the location of the fault can be obtained. Pole-to-pole (PTP) as well as PTG with a maximum 200 Ω fault resistance have been tested.

The proposed method in [30] makes use of current and voltage measurements sampled at 1 MHz to protect against DC faults on overhead lines. Discrete Wavelet Transform (DWT) is applied on pole-mode voltage and current measurements to identify the faulted pole as well as lightning disturbances for which the protection system should not react. The algorithm is configured to detect DC faults with a fault resistance up to 300 Ω.

The method introduced in [31] uses voltage measurements sampled at 500 kHz to discriminate DC faults in an overhead line-based HVDC grid. First, an under-voltage criterion on the pole-mode voltage is used as a start-up element and subsequently, DWT is applied on both pole and ground mode voltages to identify the faulted pole and line. The proposed method can detect highly-resistive faults (up to 400 Ω).

The method proposed in [32] uses an under-voltage criterion to detect every probable DC fault and the First Peak Time (FPT) of the line-mode component of the DC voltage to discriminate between internal and external faults. FPT is defined as the time instant at which the DC voltage is at its minimum. In addition, the faulted-pole is identified using the sign of the ground-mode component of the DC line voltage. For the operation of the scheme, DC voltage measurements are required with 200 kHz sampling frequency. The method has been tested for both PTP and PTG faults with faults resistances of up to 500 Ω.

The methods proposed in [33], [34], use current measurements (sampled at 200 kHz) for the first ms of the transient period of the DC fault to obtain a time-domain fitting of the fault current. The fitting coefficients are used as an indicator for discriminating between external and internal faults. Because the method fails to detect close-up faults, an under-voltage criterion is also employed to protect against such faults. The method has been tested for up to 1000 Ω fault resistance. In further work in [35], the fitting coefficients of the zero-sequence current are used to reflect the fault impedance and fault distance of PTG faults in OHL-based HVDC systems. Based on the rough estimation of these parameters, voltage derivative with an adaptive threshold is used for DC fault detection and discrimination. The method utilizes 200 kHz sampling frequency, while faults with resistance up to 300 Ω have been tested.

The proposed method in [36] utilizes current and voltage measurements captured at 110 kHz to derive the difference between the 0-mode and 1-mode surge arrival time of travelling waves. The proposed scheme has been tested for PTG faults with fault resistance of up to 200 Ω.

In [37], a generalized methodology specifically tailored for HVDC grid non-unit protection purposes is developed for flexibly deriving the key parameters for WT-based protection solutions. Among the various WT variants, Stationary Wavelet Transform (SWT) is selected and applied on DC voltage measurements (sampled at 100 kHz) to detect and discriminate between internal and external DC faults. In addition, current derivative is employed to differentiate between backward and forward faults. The method has been tested for both PTP and PTG faults, and it has been shown that it can detect internal DC faults with more than 500 Ω fault resistance.

The proposed scheme in [41] is based on instantaneous current measurements, which are obtained from all DC lines and the converter that are connected to a DC busbar. Subsequently, the measurements are analyzed through dyadic subband tree structures in order to extract specific features, such as wavelet energy, polarity, and wavelet energy ratios. The protection scheme integrates a power restoration module that re-energizes the converter and restores the power to pre-fault value.

The scheme presented in [42] utilizes local current and voltage measurements from all transmission lines connected to the same DC busbar in conjunction with DC-side converter current measurements. The proposed scheme operates at a sampling rate of 96 kHz which is compliant with IEC 61869-9. The faulted line is discriminated by wavelet transform of line voltage traces, while DC busbar faults are detected by the principle of instantaneous current differential. The scheme has been validated both for PTG and PTP faults with up to 500 Ω fault resistance.

In [43], a distance protection method is developed based on voltage and current measurements sampled at 50 kHz. The proposed solution makes use of a combined under-voltage and current derivative criterion to detect DC faults, while also the sign of the latter is used to differentiate between backward and forward faults. Discrimination between forward internal and forward external faults is accomplished by applying Hilbert-Huang Transformation (HHT) on a 4 ms data window in order to extract the DC voltage transient frequency, which in turn serves as a measure of the fault distance. The method has been tested only for PTP faults with small fault resistances.

Another method is proposed in [44] based on bus and line current measurements (50 kHz sampling frequency. The scheme requires communication on bus-level for fault discrimination and selective tripping of circuit breakers (CBs).

In [45], voltage measurements from both sides of the inductive termination are used to calculate the ratio of transient voltages and design a protection method. The method is able to achieve fault sensitivity and selectivity for solid and highly-resistive faults with fault resistances of up to 200 Ω.

The method introduced in [46] utilizes current measurements captured at 50 kHz to perform DFT and extract the high frequency components. The discrimination between external and internal faults is based on the fact that high-frequency components of the fault current flow through the faulted line and then significantly decay in adjacent healthy lines. The scheme has been tested for highly-resistive faults up to 300 Ω.

The method described in [48] is suitable for parallel-connected MTDC grids and is based upon the change rate of the current travelling waves. For the implementation of the algorithm, current and voltage measurements sampled at 50 kHz are required. In the presented studies, fault resistances of up to 100 Ω have been considered.

The non-unit method presented in [52] relies on current derivative to determine the DC fault direction and on Wavelet Transform Modulus Maxima (WTMM) of the first incident voltage travelling wave to discriminate between external and internal faults. The transfer function of the voltage at the measurement point with respect to the actual fault location is derived to calculate the protection threshold. The scheme utilizes a sampling frequency of 25 kHz and has been tested for both PTP and PTG faults with fault resistances up to 500 Ω.

The work presented in [53] utilizes voltage measurements (sampled at 25 kHz) at both sides of current-limiting inductors in bipole HVDC grids with a metallic return conductor. The rate of change is adopted to construct a directional-based

protection in order to distinguish between external and internal DC faults. The protection scheme has been tested with both PTG and PTP faults with resistance up to 200 Ω.

In [55], a two-stage approach is proposed based on current and voltage measurements to detect DC faults in multi-terminal HVDC networks. Initially, the DC fault is indicated by detecting travelling waves with the use of wavelet transform. The next stage is the fault location element that is based on the characteristic harmonic of the current. The proposed protection method utilizes very complex mathematical operations while current interruption devices and highly-resistive faults (higher than 100 Ω) are not investigated.

The method introduced in [56] utilizes voltage measurements (captured at 20 kHz) to calculate the voltage derivative, voltage change integrals and transient voltage energy. The proposed method has been tested for both PTP and PTG faults with fault resistance of up to 200 Ω.

The method presented in [57] utilizes current and voltage measurements captured at 20 kHz to calculate the current and voltage derivative, and the rate of change of the current to voltage ratio. The former two are used as start-up and security elements, while the latter is used for fault discrimination. Both PTG and to PTP faults have been tested. However, the method requires a minimum DC inductor size for its proper operation and is sensitive to highly-resistive faults.

The primary protection method described in [58] uses voltage measurements sampled at 20 kHz to discriminate DC faults in a HVDC grid with overhead lines. Initially, voltage gradient is used as a protection start-up element and then, the difference between the surge arrival time of zero-mode and line-mode travelling waves is calculated to determine the fault direction. Subsequently, voltage derivative is adopted to discriminate between forward internal and external faults. The proposed scheme has been tested for PTG and PTP faults with fault resistance up to 200 Ω.

In [59], a protection method is developed based on current measurements sampled at 20 kHz. A transformation matrix is applied on single-end current measurements of both poles to obtain the common- and differential-mode components. Subsequently, the derivative of both current components is utilized to identify the faulted pole and discriminate internal faults, while the polarity of both components is used to exclude backward faults. The method has been tested for both PTP and PTG faults with resistance up to 300 Ω.

The protection scheme introduced in [61] utilizes voltage and current measurements (captured at 10 kHz) to calculate the current and voltage derivative, under-voltage and to quantify a metric for the Current Reduction Phenomenon (CRP) (i.e. short periods in which line current reduces due to wave reflections at the fault point). Under-voltage and current derivative are initially used for fault detection and discrimination between forward/backward faults, respectively. Subsequently, voltage derivative is used as the main discrimination function and CRP is introduced to enhance the sensitivity of the method against highly-resistive faults. The method has been tested for PTP and PTG faults with a range of 0-800 Ω fault resistance.

The authors in [62] propose a non-unit protection method for HVDC grids that integrate hybrid MMCs. A DC fault is initially detected based on over-current or under-voltage (voltages and currents sampled at 10 kHz). Afterwards, the increased controllability of the hybrid MMC is exploited to inject sinusoidal signals (with different frequencies) into the DC lines of the network, and the fault distance is approximated based on a set of equations that describe the system response to the injected signals. The method is able of detecting both PTP and PTG faults with up to 200 Ω fault resistance.

The protection method proposed in [63] uses current and voltage measurements sampled at 10 kHz to detect and discriminate DC faults in hybrid LCC-VSC multiterminal systems. DWT is used to extract the required specific frequency bands of voltage and current TWs, and construct the convolution power that is used for faulted pole and fault direction identification. Moreover, convolution power-based transient energy is used to discriminate DC faults. The method has been tested for PTG and PTP faults with fault resistance up to 400 Ω.

In [64], a protection method is proposed using the median absolute deviation (MAD) of current and voltage to discriminate DC faults in multi-terminal HVDC networks. Line-side voltage and currents are sampled at 10 kHz. Nevertheless, only solid DC faults haven been investigated.

The method in [65] uses current measurements sampled at 10 kHz to apply S-Transform and extract the high and low frequency DC current components. The high frequency content is used to detect a transient event and the low frequency content is used to discriminate DC faults from other disturbances. A low voltage experimental test system has been used for the validation of the method and only low fault resistances have been considered.

In [66], real-time boundary wavelet transform (RT-BWT) is applied on voltage measurements across the series inductor (captured at 10 kHz). The algorithm is in effect a modified stationary wavelet transform that eliminates the short time delay that is commonly introduced in other WT variants. The scheme has been tested for PTP and PTG highly-resistive faults (up to 300 Ω).

The method described in [67] uses local-end DC current measurements sampled at 10 kHz. The algorithm depends on the ratio of high-to-low-frequency currents to distinguish internal from external faults. The low- (0.1–100 Hz) and high frequency (>3500 Hz) are deduced over a 5ms time window (to avoid the influence of lighting). The protection scheme detects both PTP and PTG faults with resistances of up to 200 Ω.

The proposed method in [68] relies on current measurements captured at 10 kHz to derive the transient average value of current. The method deploys analytic expressions of high-frequency equivalent models for the faulted and healthy lines to determine the thresholds for protection operation.

The scheme has been tested for both PTG and PTP faults with fault resistance of up to 500 Ω.

The scheme presented in [69] calculates the high frequency transient-voltage energy to determine the faulted section (external or internal fault). The method deploys the Mallat algorithm to extract the detailed coefficients at a specific decomposition level and then the peak energy of the detailed coefficients is obtained. Voltage measurements are captured at 10 kHz while the proposed scheme has been tested for both PTP and PTG faults with fault resistance of up to 300 Ω.

The scheme presented in [71] is based on artificial neural networks (ANN). In this scheme, high frequency fault current components are input to ANNs, where they are analyzed in the frequency domain to extract the signal's spectral components. The protection scheme has been tested for PTG and PTP faults with resistance of up to 100 Ω. The algorithm operates within a 6-ms time window with signals sampled at 10 kHz.

The method proposed in [73] is based on a Naïve Bayes classifier, which is utilized to determine voltage and current thresholds and define the operational time frames for both primary and back-up protection. The proposed scheme requires DC voltage and current measurements sampled at 10 kHz. The performance of the method has been tested for PTP faults with resistance up to 10 Ω while PTG DC faults have not been investigated or analyzed at all.

The method described in [74] uses the average value of the fault line current to detect and discriminate DC faults in radial HVDC networks. Moreover, a simplified transient model is developed and used for the calculation of the protection threshold. Current measurements are only required for this scheme and the sampling frequency is set to 10 kHz.

The scheme presented in [78] is a four-stage protection algorithm based on DC over-current, DC current derivative, Wavelet Transform, Principal Component Analysis (PCA), and a Genetic Fuzzy System (GFS). The system utilizes current measurements sampled at 2 kHz and requires no communication. The scheme performance has been validated for resistance of up to 50 Ω, however after such value its response seems to be compromised. Another significant drawback of this method is the fact that it depends on complicated and numerous mathematical operations, while there is a need for a training data base.

The method in [82] utilizes local voltage measurements at either side of current limiting inductors (sampled at 8 kHz) to implement a basic directional element. The same principle is used to develop a slower communication-based DC line protection scheme for detecting highly-resistive faults up to 200 Ω.

In [83], the handshaking method is proposed to detect the DC line in which a fault has occurred. Nevertheless, the method is considered to be relatively slow and AC breakers are used for DC fault isolation (which can take several AC cycles and therefore tenths of ms to operate) leading to de-energization of the DC grid.

Travelling wave principles are used in [84] to design a method that utilizes DC voltage and current derivatives to determine whether the fault is external or internal. Nevertheless, this method can be very sensitive to noise and may lead to false protection operation.

The detection method in [85] utilizes a three-stage approach and a voting scheme to identify and discriminate the existence and location of faults. The stages include wavelet analysis of DC voltages and currents, as well as voltage derivative and amplitude. However, PTG faults have not been investigated while the protection algorithm appears to be relatively complex and dependent on many parameters, and may therefore be impractical to implement.

In [86], a primary and secondary protection scheme is proposed. The primary scheme utilizes the voltage across the inductors of both positive and negative DC poles. A trigger is initiated by an under-voltage criterion on any of the reactor voltages. Further fault classification is achieved by calculating the differential voltage of the two DC reactors. A back-up scheme is introduced to account for highly-resistive faults. In this case, voltage from both line terminals are required and as such communication is required. Using voltages from both sides, a directional and a magnitude element are calculated from which the fault is detected and classified. In the studies presented the DC reactor size is set to 150 mH and the proposed scheme works for DC reactors of up to 30 mH. The needs of sampling frequency have not been specified. In the presented studies resistances of up to 1000 Ω have been considered.

The method described in [87] uses distributed sensors integrated in cable joints to provide and construct voltage and current-based superimposed elements. The method combines a protection algorithm together with proactive hybrid breakers to increase the speed of operation and achieve increased performance. The algorithm has been tested for both PTG and PTP faults with fault resistances in the range of hundreds of ohms. The sampling frequency and time window requirements haven't been specified.

The protection strategy proposed in [88] relies on DC current and voltage measurements. The proposed strategy uses AC-side CBs to clear DC-side faults and rapid DC disconnectors for fault isolation. DC-side faults are detected by over-current or under-voltage criteria while the faulted line is discriminated based on two criteria employing DC current magnitude and sign. The method is capable of detecting both PTG and PTP faults. However, the sampling frequency needs are not specified while highly-resistive faults have not been investigated.

The method described in [89] deploys local current and voltage measurements to realize a protection scheme based on under-voltage, voltage derivative and current derivative. The scheme presented in [54] relies on current and measurements (sampled at 20 kHz) to carry out frequency-spectrum correlation and identify the faulted line.

In [93], a protection scheme of overhead line-based HVDC grids is proposed. First, voltage derivative is used as

a start-up element to activate the protection scheme followed by the calculation of the integral of the line-mode and ground-mode components of the voltage across the DC reactor in order to identify the faulted pole and to discriminate internal faults, respectively. PTP and PTG faults with fault resistances of up to 200 Ω are tested.

The protection scheme introduced in [94], uses current magnitude and current derivative to calculate the current limiting reactor power (CLRP). A back-up protection based on the direction of both currents of the transmission line is also employed to protect against highly-resistive faults.

In [188], a travelling-wave based direction criterion has been presented that uses DWT to obtain the high frequency content of DC voltage and current traces in order to distinguish between backward and forward faults. The sampling frequency of this method can be flexibly selected, and 10 kHz was used for illustration. The sensitivity of the method for forward faults with up to 300 Ω fault resistance has been demonstrated.

UNIT

There is also a significant number of differential type protection schemes proposed in the open literature [29], [39], [40], [76], [90], [91]. Some of the main drawbacks and challenges associated with differential protection include the delays associated with encoding and decoding messages, its inherent communication time delays, the need for communication path latency corrections, and its reliability especially when one of the measurements is lost or the communications link is compromised.

In [39] a combined scheme is proposed, which is based on polarity comparison of initial current travelling wave (for line faults) and on sampled value current differential theory (for DC busbar faults). DC currents (sampled at 100 kHz) from two line ends are utilized to distinguish between internal and external faults by applying the WTMM theory on current travelling waves. Current differential protection based on sampled values is achieved over 5 consecutive sampling points at 10 kHz. In the presented studies resistances of up to 400 Ω and resistive superconducting fault current limiters (R-SFCLs) have been used.

In [40], current signals at both line ends are captured and processed by DWT in the main protection algorithm. In detail, certain DWT components that are extracted from current signals processing at both ends are used to perform energy comparison and achieve discrimination between internal and external faults.

The method presented in [50] uses the energy of DWT coefficients derived from line current measurements sampled at 50 kHz. Moreover, a change in current direction from at least one of the medium ends needs to be identified in order to detect an internal fault. Only low resistive PTP faults are investigated in this study.

The authors in [51] use voltage gradient to detect a DC fault and comparison of the polarities of the voltage across the DC reactors on both ends of an overhead line to discriminate between external and internal faults. The selected sampling rate is 50 kHz. The integral of the DC reactor voltage is used to obtain the polarity. The method has been tested for PTP and PTG fault, and it has been shown that it can identify DC faults with 400 Ω fault resistance.

In the unit protection scheme that is proposed in [60], the ratio of transient energy (TER) is calculated at both sides of the protected medium and used as the main protection element. The method has been tested for LCC-based HVDC systems using current and voltage measurements sampled at 20 kHz. In the presented studies, resistances of up to 1000 Ω have been tested.

In [72], a communication-based scheme is proposed based on similarity measure of travelling waves. The proposed scheme utilizes voltage and current measurements at both transmission line ends, which are analyzed to derive the cosine similarity of backward and forward travelling waves. The scheme has been tested with fault resistances of up to 1000 Ω.

The unit protection method introduced in [75] uses current and voltage measurements (with 20 kHz sampling frequency) of both ends of a transmission line to calculate the differential voltage travelling wave in the time domain by means of convolution. A method to compensate for out-of-sync data measurements from the two sides of the line is provided. Moreover, a comprehensive analysis of all sources of time delay is realized to obtain a total delay time estimation formula. The method has been tested for PTG and PTP faults.

In [76], distributed current sensors are placed along the transmission lines of the HVDC system in order to implement a high-speed differential scheme. In the presented studies, the method has been found to be sensitive, fast, stable during external faults and reliable for both solid and highly-resistive internal DC faults.

The authors in [77] use voltage and current measurements sampled at 5 kHz to develop a unit protection method. Cosine Distance (CD) is utilized as a metric of similarity between the analyzed signal and a pre-recorded reference signal to detect forward DC faults. A fault is identified as internal, when the local protective relay detects a DC fault, and a fault detection signal is received from the protective relay at the remote end of the protection zone. Highly-resistive (up to 100 Ω) PTP and PTG faults have been considered.

A phase-domain travelling wave differential protection is presented in [79], in which transmission line models have been developed for the application of the protection scheme using only information contained in the first travelling wave. It is worth noting that the required communication and wave propagation have the same direction, resulting in smaller communication delays than conventional unit protection methods. In addition, a sensitivity analysis of the cable parameters has been realized in [189] to investigate the impact of potential sources of error on the protection scheme.

The differential protection scheme that is proposed in [90] performs a comparison between the currents of line terminals for fault discrimination, while fault isolation is performed

using mechanical DC breakers. Nevertheless, such methods rely on the use of fault-tolerant converters in order to allow for low-speed fault isolation. Moreover, the protection algorithm is essentially based on a single criterion with a fixed predefined threshold. The lack of other criteria raises concerns regarding the reliability of the algorithm against noise and measurement uncertainties.

BACKUP

Even though numerous unit and non-unit primary relaying algorithms have been proposed, the need for backup relaying is always inevitable. Such schemes can ensure system reliability when the primary systems fail to operate. Primary systems might fail due to several reasons such as failure of the communication link, transducers or the protection algorithm itself.

The main principle of the algorithm presented in [47] is based on voltage and current response associated with DC breaker operation (instead of the wide-system characteristics). The approach is based on fault classification in the V/I locus for cleared but also for non-cleared faults across the network. The system requires training data and takes into account both CB and relay failures. The proposed scheme provides efficient backup protection, but further studies have to be implemented considering acceptable levels of noise, sampling frequency and resistive faults.

The underlying theory of the proposed back-up scheme in [49] is to determine the status of the primary relay and breakers by monitoring any abrupt change at the terminal voltage and breaker voltage respectively (captured at 50 kHz). The algorithm is based on the quickest change detection based on the maximum likelihood principle (applied on the log-likelihood ratio).

The method in [70] utilizes local current measurements captured at 10 kHz to decompose and extract wavelet packets. The Shannon entropy theorem is deployed to calculate the Wavelet-Packet Energy Entropy (WPEE) and discriminate between external and internal faults. The scheme has been tested on PTP and PTGs faults with fault resistances of up to 1000 Ω.

A similar method based on V/I locus can also be found in [92]. However, the sampling frequency needs have not been specified, while primary protection system failures in case of PTG faults have not been considered at all.

APPENDIX B
DETAILED REVIEW ON FAULT LOCATION METHODS

TRAVELLING WAVES

During transmission line faults, due to the abrupt change in voltage, a series of transients are generated which travel along the lines in all directions. These transients are known as travelling waves and they have some unique features such as polarity, magnitude, and time intervals [98].

In several technical publications, it has been demonstrated that travelling wave principles can be used to estimate the fault position on a transmission medium with high accuracy. Fault location estimation based on TWs can be achieved using measurements either from a single end or from both ends of the faulted medium. In single-ended methods, two consecutive TW reflections are required to be captured using measurements at one terminal, while in two-ended methods, only the first reflection needs to be captured at both line terminals using synchronized time-stamped measurements. Since, the first reflection provides the least attenuated signature, two-ended methods are generally considered more reliable [96]. Nevertheless, the selection between single- and two-ended methods is a trade-off between complexity, reliability, cost and required accuracy of the estimation [108]. Based on TWs, several methods have been proposed, by utilizing different mathematical tools to extract specific features from voltage and/or current signals.

In [95], a fault location method is proposed for star connected MTDC networks using wavelet transform. In detail, the method is based on the application of continuous wavelet transform (CWT) on DC line current signals, and it has been shown to be capable of eliminating the requirement for repeater stations at the network junctions. Nevertheless, time-synchronized measurements and a high sampling frequency of 2 MHz are required. Moreover, highly-resistive DC faults have not been investigated thoroughly.

Authors in [96] propose a two-ended TW-based fault location method using time-stamped measurements (sampled at 2 MHz) of DC voltage and capacitor currents to locate DC faults in HVDC networks with non-homogeneous transmission media. Initially, the faulty segment is identified by solving a set of equations for calculating the fault distance for each segment. The method is accurate and robust against noise, nevertheless, only fault resistances up to 100 Ω were investigated. Moreover, the requirement for synchronized measurements and high sampling frequency could be considered a barrier for practical applications.

TWs together with HHT are also used in a fault location method for hybrid LCC-MMC HVDC systems that is proposed in [97]. HHT is used to obtain the amplitude-frequency coefficients and calculate the arrival time of the voltage travelling waves at all terminals. Then the arrival times are used to estimate the fault distance. The method uses voltage measurements with 1 MHz sampling frequency, and it has been tested for DC faults with fault resistance up to 300 Ω.

In [98], the basic principle of single-ended TW-based fault location together with two graph theory-based lemmas together are utilized to locate DC faults in MTDC networks. The method is robust against network topology and high impedance faults. However, high sampling frequency is required (1 MHz), while detection of the first wave-front could be challenging [108].

TWs together with HHT and Ensemble Empirical Mode Decomposition (EEMD) are used in a fault location method that is proposed in [99]. The HHT and EEMD are used to obtain the time-frequency graph from which the arrival time of the waves and the corresponding instantaneous frequency

are derived. The propagation velocity is then calculated (by using the instantaneous frequency) and together with the arrival time a two-ended technique is used to calculate the fault distance. The sampling requirement of this method is 1 MHz while highly-resistive faults have not been investigated.

A flexible TW-based protection is proposed in [100] which can either adopt single or two-ended fault location approach to accurately estimate the location of the fault. Nevertheless, the proposed idea requires TW data acquisition centers, repeater stations and communication links between them, which obviously increase the cost and complexity, while the reliability could be low. Voltage and current measurements are sampled at 1 MHz.

In [101], modal currents and voltages are used to implement a single-ended travelling-wave based fault location method for HVDC cable bundles. The method requires voltages and currents sampled at 1 MHz, and it has been tested with fault resistance of up to 100 Ω.

A TW-based method eliminating the need for synchronized measurements and the information of line parameters is proposed [102]. The method requires two-end voltage and current measurements to construct a time-domain fault location method. This is achieved by combing the Bergeron line model together with TW principles (with the zero time reference adjusted to the surge arrival point at each end). The proposed method can locate both solid and high impedance faults (up to 500 Ω) with good accuracy, however a high sampling frequency is needed (1 MHz).

The method introduced in [33] utilizes current measurements sampled at 200 kHz to implement a single-ended TW-based fault location algorithm. The proposed method utilizes the Generalized Logistic Function (GLF) to extract the fault information and a Predictor-Corrector (PC) fault location component to compensate for errors. The scheme has been tested with fault resistance of up to 300 Ω.

Compared to the conventional TW-based fault location methods, the proposed method presented in [105] eliminates the need to accurately estimate the arrival time of the waves. The proposed idea utilizes the dominant natural frequency in the spectrum analysis of TW (also known as natural frequency), which is used to calculate the wave velocity, reflection coefficients and reflection angles, and then estimate fault location. The method requires voltages and currents only from one end while a sampling frequency of 100 kHz is required. However, the method has been tested for high impedance faults of only up to 50 Ω.

All methods based on TWs require high sampling frequency in order to achieve high accuracy on the estimation of the fault location [95]. Such requirement is frequently considered as an important drawback of TW-based methods. Additional challenges include the first wave detection [108], the need for synchronized measurements [96], and the fact that the propagation speed of the transmission medium should be known [96]. The propagation speed theoretical value can be either deduced by the conductor geometry or estimated by a known fault location. Such data can be obtained during the commissioning process of the fault locator system.

IMPEDANCE-BASED

Even though impedance-based methods are well established in AC systems [190], it is quite impractical to implement them in HVDC lines because of the lack of a fundamental frequency. A few approaches have been proposed in the open literature, where the line impedance estimation is adopted. However, due to their nature they fall under the category of refractometry presented below.

REFLECTOMETRY

The main idea of refractometry is to inject short-time signals into the faulted line and based on the detected response and captured current and voltage signatures, the fault location can be estimated. Fault location methods based on reflectometry can be also found in the literature under the term 'active methods'. Such methods require the use of external equipment, which is usually surge pulse generators and a set of detectors. Depending on the selected approach, such methods resemble the use of TW-based and impedance-based methods. In particular Time Domain Reflectometry (TDR), Impulse Current Method (ICM), Multiple Impulse Method (MIM), Secondary Impulse Method (SIM), Decay Method (DM), Impulse Current Differential Method (ICDM) and Differential Decay Method (DDM) use the same principle as TW-based methods, which is the surge arrival time calculation. On the other hand, impedance-based methods utilize current and voltage measurements from which the impedance and consequently the fault location is calculated.

In [110], a DC circuit breaker is used as means to inject a DC voltage pulse (around 10 kV) and then implement a single-ended type fault location method. The method is based on voltage measurements sampled at 50 kHz, which results in approximately ±3 km estimation errors. The proposed method has been tested with fault resistance of up to 100 Ω.

In [191], a fault location algorithm based on stationary wavelet transform is proposed. The injected high-frequency signals are captured by an oscilloscope, decomposed by wavelet transform and rescaled by multiple-scale correlation of approximations. Finally, the actual fault location is estimated through the time delay between two consecutive incidents.

In [192], an improved fault localization technique is proposed which is based on time-frequency domain reflectometry in addition to tangent distance pattern recognition. The method requires a signal generator to inject reference signals into submarine cables. The reflected signal is then captured and together with the reference signal are used for post-fault analysis by adopting time-frequency distribution, Euclidean and tangent distance. The method has been validated practically on a section of a HVDC cable and has been found to be accurate. However, the sampling rate for reference and reflected signals is 8 GHz and 312.5 MHz respectively, and requires special and possibly expensive equipment.

In addition, the analysis requires a series of multiple and complex mathematical operations and the influence of fault resistance has not been investigated at all. For further research on reflectometry-based techniques, the literature in [193] may be consulted.

LEARNING-BASED METHODS

A unique category among fault location approaches includes the application of learning-based tools. Despite the fact that such techniques are widely used in fault classification and localization in AC systems, there is a limited number of available publications addressing their applicability to HVDC networks [103], [104], [106]–[108], [112], [114].

In [103] a method based on extreme learning machine (ELM) is proposed to locate DC faults in MTDC HVDC systems. S-transform and wavelet transform are employed for extracting the features to be used in the learning process. The method requires voltage and current measurements sampled at 500 kHz and the entire scheme has been tested for faults with resistance of up to 100 Ω.

In [104], a learning-based approach is introduced for segmented transmission lines (lines that consist of more than one cable/OHL segments). Initially, DWT is applied on current and voltage signals (sampled at 200 kHz) to obtain the wavelet energies, which are then input to a support vector machine (SVM) classifier to determine the faulted segment. Finally, traditional single-ended TW analysis is used in order to estimate the fault location. It is worth noting that the method is limited to transmission media with only two segments and that highly-resistive faults have not been investigated.

The method in [106] is based on non-synchronous voltage measurements captured at 100 kHz on both line ends. The proposed method utilizes Empirical Mode Decomposition (EMD) to extract the high-frequency component in the fault signal and then Convolutional Neural Network (CNN) to classify the data and estimate the fault location. The method has been tested for both PTG and PTP faults and it was demonstrated that it can reliably and accurately estimate the fault distance even with a fault resistance of 5200 Ω.

The method in [107] utilizes DC current measurements (sampled at 96 kHz) from hybrid DC breakers to identify switching patterns and locate the fault along OHLs and cables. The method has been found to be accurate for all types of faults with fault resistances of up to 500 Ω.

A learning-based method on post-fault voltage measurements with 80 kHz sampling frequency is proposed in [108]. The fault location scheme estimates the fault distance by calculating the Pearson correlation coefficients between existing cases (with unknown fault location) and pre-simulated voltage patterns. The method has been found to be accurate for long transmission lines and for different types of faults. However, it has been tested only for high impedance faults up to 80 Ω, while obtaining a data base of training patterns can always be challenging.

A method based on a network of distributed sensors is proposed in [112]. The method utilizes current measurements obtained at 5 kHz to apply a conventional two-ended TW-based fault location technique. A machine learning approach is then used to reduce the distance error arising from the moderate sampling frequency.

The method in [114] is based on a SVM regression algorithm to estimate the location of a fault on a DC line. The method requires AC voltage, DC voltage and DC current measurements obtained at 1 kHz or 4 kHz (half cycle pre-fault and post-fault data are used). The method has been tested for both PTP and PTG faults, however high impedance faults have not been investigated.

OTHER METHODS

In an effort to overcome the practical challenges related to the application of TW-based methods, a few other schemes can be found in the technical literature.

A fault location method for HVDC grids based on a simplified R-L line model for representing transmission lines with reduced computational burden is proposed in [109]. A fault location coefficient (FLC) is obtained through the simplified R-L model and used to calculate the fault distance. The method uses current and voltage measurements sampled at 50 kHz for a 5 ms time window and it has been tested for high impedance faults (500 Ω).

In [111], another method based on post-fault data is proposed. Specifically, by using current and voltage measurements from both line sides (synchronized), the voltage distribution across the Bergeron line model is calculated and the fault distance is estimated. The required sampling frequency is 6.4 kHz and the method has been found to be accurate in locating DC faults in long transmission lines and with high fault resistances (up to 500 Ω).

In [113] an improved electromagnetic time-reversal (EMTR)-based method is proposed. The method is based on the mathematical formulation of EMTR to lossless lines and requires current measurements captured at 5 kHz. The performance of the method has been tested for both PTP and PTG faults and for resistances of up to 800 Ω.

REFERENCES

[1] B. Moselle, J. Padilla, and R. Schmalensee, *Harnessing Renewable Energy in Electric Power Systems Theory, Practice, Policy*. Washington, DC, USA: RFF Press, 2010.
[2] "European offshore supergrid proposal," Airtricity, Dublin, Ireland, Tech. Rep., 2006. [Online]. Available: http://www.desertec-uk.org.uk/resources/airtricity_supergrid_V1.4.pdf
[3] Friends of the Supergrid, "Position paper on the EC communication for a european infrastructure package—Phase 1," Friends Supergrid, Brussels, Belgium, Tech. Rep. 12/2010, Dec. 2010.
[4] European Wind Energy Association, "Powering Europe: Wind energy and the electricity grid," European Wind Energy Assoc., Brussels, Belgium, Tech. Rep. 11/2010, Nov. 2010.
[5] OffShoreGrid, "Offshore electricity grid infrastructure in Europe," OffShoreGrid, Brussels, Belgium, Final Rep., Oct. 2011.
[6] D. V. Hertem, O. Gomis-Bellmunt, and J. Liang, *HVDC Grids for Offshore and Supergrid of The Future*. Hoboken, NJ, USA: Wiley, 2016.
[7] D. Van Hertem and M. Ghandhari, "Multi-terminal VSC HVDC for the European supergrid: Obstacles," *Renew. Sustain. Energy Rev.*, vol. 14, no. 9, pp. 3156–3163, Dec. 2010.

[8] G. Zarazua de Rubens and L. Noel, "The non-technical barriers to large scale electricity networks: Analysing the case for the US and EU supergrids," *Energy Policy*, vol. 135, Dec. 2019, Art. no. 111018.

[9] D. Bogdanov and C. Breyer, "North-East Asian super grid for 100% renewable energy supply: Optimal mix of energy technologies for electricity, gas and heat supply options," *Energy Convers. Manage.*, vol. 112, pp. 176–190, Mar. 2016.

[10] Y. Lei, Y. Lu, Y. Li, Y. Liu, K. Tomsovic, and F. Wang, "A preliminary study of building a transmission overlay for regional U.S. power grid," in *Proc. IEEE Power Energy Soc. Gen. Meeting*, Jul. 2015, pp. 1–5.

[11] J. A. Ansari, C. Liu, and S. A. Khan, "MMC based MTDC grids: A detailed review on issues and challenges for operation, control and protection schemes," *IEEE Access*, vol. 8, pp. 168154–168165, 2020.

[12] B. Chang, O. Cwikowski, M. Barnes, R. Shuttleworth, A. Beddard, and P. Coventry, "Review of different fault detection methods and their impact on pre-emptive VSC-HVDC DC protection performance," *High Voltage*, vol. 2, no. 4, pp. 211–219, Dec. 2017.

[13] T.-C. Peng, D. Tzelepis, A. Dysko, and I. Glesk, "Assessment of fault location techniques in voltage source converter based HVDC systems," in *Proc. IEEE Texas Power Energy Conf. (TPEC)*, Feb. 2017, pp. 1–6.

[14] W. Wang and M. Barnes, "Power flow algorithms for multi-terminal VSC-HVDC with droop control," *IEEE Trans. Power Syst.*, vol. 29, no. 4, pp. 1721–1730, Jul. 2014.

[15] J. Beerten, S. Cole, and R. Belmans, "Generalized steady-state VSC MTDC model for sequential AC/DC power flow algorithms," *IEEE Trans. Power Syst.*, vol. 27, no. 2, pp. 821–829, May 2012.

[16] J. Lei, T. An, Z. Du, and Z. Yuan, "A general unified AC/DC power flow algorithm with MTDC," *IEEE Trans. Power Syst.*, vol. 32, no. 4, pp. 2837–2846, Jul. 2017.

[17] A. Raza, X. Dianguo, L. Yuchao, S. Xunwen, B. W. Williams, and C. Cecati, "Coordinated operation and control of VSC based multiterminal high voltage DC transmission systems," *IEEE Trans. Sustain. Energy*, vol. 7, no. 1, pp. 364–373, Jan. 2016.

[18] E. Prieto-Araujo, A. Egea-Alvarez, S. Fekriasl, and O. Gomis-Bellmunt, "DC voltage droop control design for multiterminal HVDC systems considering AC and DC grid dynamics," *IEEE Trans. Power Del.*, vol. 31, no. 2, pp. 575–585, Apr. 2016.

[19] L. Xiao, Z. Xu, T. An, and Z. Bian, "Improved analytical model for the study of steady state performance of droop-controlled VSC-MTDC systems," *IEEE Trans. Power Syst.*, vol. 32, no. 3, pp. 2083–2093, May 2017.

[20] E. Rakhshani, D. Remon, A. M. Cantarellas, J. M. Garcia, and P. Rodriguez, "Virtual synchronous power strategy for multiple HVDC interconnections of multi-area AGC power systems," *IEEE Trans. Power Syst.*, vol. 32, no. 3, pp. 1665–1677, May 2017.

[21] Y. Pipelzadeh, N. R. Chaudhuri, B. Chaudhuri, and T. C. Green, "Coordinated control of offshore wind farm and onshore HVDC converter for effective power oscillation damping," *IEEE Trans. Power Syst.*, vol. 32, no. 3, pp. 1860–1872, May 2017.

[22] M. Andreasson, R. Wiget, D. V. Dimarogonas, K. H. Johansson, and G. Andersson, "Distributed frequency control through MTDC transmission systems," *IEEE Trans. Power Syst.*, vol. 32, no. 1, pp. 250–260, Jan. 2017.

[23] N. A. Belda, C. A. Plet, and R. P. P. Smeets, "Analysis of faults in multiterminal HVDC grid for definition of test requirements of HVDC circuit breakers," *IEEE Trans. Power Del.*, vol. 33, no. 1, pp. 403–411, Feb. 2018.

[24] M. N. Haleem and A. D. Rajapakse, "Fault-type discrimination in HVDC transmission lines using rate of change of local currents," *IEEE Trans. Power Del.*, vol. 35, no. 1, pp. 117–129, Feb. 2020.

[25] D. Tzelepis, G. Fusiek, A. Dysko, P. Niewczas, C. Booth, and X. Dong, "Novel fault location in MTDC grids with non-homogeneous transmission lines utilizing distributed current sensing technology," *IEEE Trans. Smart Grid*, vol. 9, no. 5, pp. 5432–5443, Sep. 2018.

[26] ENTSOE-E, "Establishing a network code on requirements for grid connection of high voltage direct current systems and direct current-connected power park modules," *Off. J. Eur. Union*, vol. 2, pp. 1–65, Aug. 2016.

[27] *IEEE Guide for Establishing Basic Requirements for High-Voltage Direct-Current Transmission Protection and Control Equipment*, IEEE Standard 1899-2017, Jun. 2017, pp. 1–47.

[28] K. A. Saleh, A. Hooshyar, E. F. El-Saadany, and H. H. Zeineldin, "Protection of high-voltage DC grids using traveling-wave frequency characteristics," *IEEE Syst. J.*, vol. 14, no. 3, pp. 4284–4295, Sep. 2020.

[29] J. Descloux, P. Rault, S. Nguefeu, J. B. Curis, X. Guillaud, F. Colas, and B. Raison, *HVDC Meshed Grid: Control and Protection of a Multi-Terminal HVDC System*. Paris, France: CIGRE, 2012.

[30] L. Tang, X. Dong, S. Shi, and Y. Qiu, "A high-speed protection scheme for the DC transmission line of a MMC-HVDC grid," *Electr. Power Syst. Res.*, vol. 168, pp. 81–91, Mar. 2019.

[31] X. Pei, H. Pang, Y. Li, L. Chen, X. Ding, and G. Tang, "A novel ultra-high-speed traveling-wave protection principle for VSC-based DC grids," *IEEE Access*, vol. 7, pp. 119765–119773, 2019.

[32] C. Zhang, G. Song, and X. Dong, "Non-unit Ultra-high-speed DC line protection method for HVDC grids using first peak time of voltage," *IEEE Trans. Power Del.*, early access, Jul. 30, 2020, doi: 10.1109/TPWRD.2020.3013021.

[33] C. Zhang, G. Song, T. Wang, and L. Yang, "Single-ended traveling wave fault location method in DC transmission line based on wave front information," *IEEE Trans. Power Del.*, vol. 34, no. 5, pp. 2028–2038, Oct. 2019.

[34] C. Zhang, G. Song, T. Wang, L. Wu, and L. Yang, "Non-unit traveling wave protection of HVDC grids using Levenberg-Marquart optimal approximation," *IEEE Trans. Power Del.*, vol. 35, no. 5, pp. 2260–2271, Oct. 2020.

[35] C. Zhang, G. Song, T. Wang, and X. Dong, "An improved non-unit traveling wave protection method with adaptive threshold value and its application in HVDC grids," *IEEE Trans. Power Del.*, vol. 35, no. 4, pp. 1800–1811, Aug. 2020.

[36] N. Tong, X. Lin, Y. Li, Z. Hu, N. Jin, F. Wei, and Z. Li, "Local measurement-based Ultra-High-Speed main protection for long distance VSC-MTDC," *IEEE Trans. Power Del.*, vol. 34, no. 1, pp. 353–364, Feb. 2019.

[37] V. Psaras, D. Tzelepis, D. Vozikis, G. Adam, and G. Burt, "Non-unit protection for HVDC grids: An analytical approach for wavelet transform-based schemes," *IEEE Trans. Power Del.*, early access, Sep. 18, 2020, doi: 10.1109/TPWRD.2020.3024818.

[38] W. Leterme, J. Beerten, and D. Van Hertem, "Nonunit protection of HVDC grids with inductive DC cable termination," *IEEE Trans. Power Del.*, vol. 31, no. 2, pp. 820–828, Apr. 2016.

[39] G. Zou, Q. Feng, Q. Huang, C. Sun, and H. Gao, "A fast protection scheme for VSC based multi-terminal DC grid," *Int. J. Electr. Power Energy Syst.*, vol. 98, pp. 307–314, Jun. 2018.

[40] A. E. B. Abu-Elanien, A. A. Elserougi, A. S. Abdel-Khalik, A. M. Massoud, and S. Ahmed, "A differential protection technique for multi-terminal HVDC," *Electr. Power Syst. Res.*, vol. 130, pp. 78–88, Jan. 2016.

[41] D. Tzelepis, S. M. Blair, A. Dysko, and C. Booth, "DC busbar protection for HVDC substations incorporating power restoration control based on dyadic sub-band tree structures," *IEEE Access*, vol. 7, pp. 11464–11473, 2019.

[42] D. Tzelepis, A. Dyśko, S. M. Blair, A. O. Rousis, S. Mirsaeidi, C. Booth, and X. Dong, "Centralised busbar differential and wavelet-based line protection system for multi-terminal direct current grids, with practical IEC-61869-compliant measurements," *IET Gener., Transmiss. Distrib.*, vol. 12, no. 14, pp. 3578–3586, Aug. 2018.

[43] V. Albernaz Lacerda, R. M. Monaro, D. Campos-Gaona, D. V. Coury, and O. Anaya-Lara, "Distance protection algorithm for multiterminal HVDC systems using the Hilbert–Huang transform," *IET Gener., Transmiss. Distrib.*, vol. 14, no. 15, pp. 3022–3032, 2020.

[44] S. Pirooz Azad and D. Van Hertem, "A fast local bus current-based primary relaying algorithm for HVDC grids," *IEEE Trans. Power Del.*, vol. 32, no. 1, pp. 193–202, Feb. 2017.

[45] J. Liu, N. Tai, and C. Fan, "Transient-Voltage-Based protection scheme for DC line faults in the multiterminal VSC-HVDC system," *IEEE Trans. Power Del.*, vol. 32, no. 3, pp. 1483–1494, Jun. 2017.

[46] Y. Li, L. Wu, J. Li, L. Xiong, X. Zhang, G. Song, and Z. Xu, "DC fault detection in MTDC systems based on transient high frequency of current," *IEEE Trans. Power Del.*, vol. 34, no. 3, pp. 950–962, Jun. 2019.

[47] W. Leterme, S. Pirooz Azad, and D. Van Hertem, "A local backup protection algorithm for HVDC grids," *IEEE Trans. Power Del.*, vol. 31, no. 4, pp. 1767–1775, Aug. 2016.

[48] J. Cheng, X. Chen, H. Huang, J. Xie, L. Tang, and M. Guan, "Paralleled multi-terminal DC transmission line fault locating method based on travelling wave," *IET Gener., Transmiss. Distrib.*, vol. 8, no. 12, pp. 2092–2101, Dec. 2014.

[49] J. Sun, M. Saeedifard, and A. P. S. Meliopoulos, "Backup protection of multi-terminal HVDC grids based on quickest change detection," *IEEE Trans. Power Del.*, vol. 34, no. 1, pp. 177–187, Feb. 2019.
[50] B. Mitra, B. Chowdhury, and A. Willis, "Protection coordination for assembly HVDC breakers for HVDC multiterminal grids using wavelet transform," *IEEE Syst. J.*, vol. 14, no. 1, pp. 1069–1079, Mar. 2020.
[51] Q. Huang, G. Zou, S. Zhang, and H. Gao, "A pilot protection scheme of DC lines for multi-terminal HVDC grid," *IEEE Trans. Power Del.*, vol. 34, no. 5, pp. 1957–1966, Oct. 2019.
[52] S. Zhang, G. Zou, C. Wang, J. Li, and B. Xu, "A non-unit boundary protection of DC line for MMC-MTDC grids," *Int. J. Electr. Power Energy Syst.*, vol. 116, Mar. 2020, Art. no. 105538.
[53] N. M. Haleem and A. D. Rajapakse, "Local measurement based ultra-fast directional ROCOV scheme for protecting bi-pole HVDC grids with a metallic return conductor," *Int. J. Electr. Power Energy Syst.*, vol. 98, pp. 323–330, Jun. 2018.
[54] K. Zhu, W. K. Lee, and P. W. T. Pong, "Fault-line identification of HVDC transmission lines by frequency-spectrum correlation based on capacitive coupling and magnetic field sensing," *IEEE Trans. Magn.*, vol. 54, no. 11, pp. 1–5, Nov. 2018.
[55] J. Cheng, M. Guan, L. Tang, and H. Huang, "A fault location criterion for MTDC transmission lines using transient current characteristics," *Int. J. Electr. Power Energy Syst.*, vol. 61, pp. 647–655, Oct. 2014.
[56] W. Xiang, S. Yang, L. Xu, J. Zhang, W. Lin, and J. Wen, "A transient voltage-based DC fault line protection scheme for MMC-based DC grid embedding DC breakers," *IEEE Trans. Power Del.*, vol. 34, no. 1, pp. 334–345, Feb. 2019.
[57] M. Elgeziry, M. Elsadd, N. Elkalashy, T. Kawady, A. Taalab, and M. A. Izzularab, "Non-pilot protection scheme for multi-terminal VSC–HVDC transmission systems," *IET Renew. Power Gener.*, vol. 13, no. 16, pp. 3033–3042, 2019.
[58] X. Yu and L. Xiao, "A DC fault protection scheme for MMC-HVDC grids using new directional criterion," *IEEE Trans. Power Del.*, early access, Mar. 2, 2020, doi: 10.1109/TPWRD.2020.2977373.
[59] J. Liao, N. Zhou, and Q. Wang, "DC grid protection method based on phase planes of single-end Common- and differential-mode components," *IEEE Trans. Power Del.*, early access, Feb. 27, 2020, doi: 10.1109/TPWRD.2020.2976721.
[60] Z. Dai, N. Liu, C. Zhang, X. Pan, and J. Wang, "A pilot protection for HVDC transmission lines based on transient energy ratio of DC filter link," *IEEE Trans. Power Del.*, vol. 35, no. 4, pp. 1695–1706, Aug. 2020.
[61] T. Lan, Y. Li, and X. Duan, "High fault-resistance tolerable traveling wave protection for multi-terminal VSC-HVDC," *IEEE Trans. Power Del.*, early access, May 28, 2020, doi: 10.1109/TPWRD.2020.2998158.
[62] G. Song, J. Hou, B. Guo, S. T. H. Kazmi, T. Wang, and B. Masood, "Active injection for single-ended protection in DC grid using hybrid MMC," *IEEE Trans. Power Del.*, early access, Jul. 29, 2020, doi: 10.1109/TPWRD.2020.3012779.
[63] X. Chen, H. Li, G. Wang, C. Xu, and Y. Liang, "A convolution power-based protection scheme for hybrid multiterminal HVDC transmission systems," *IEEE J. Emerg. Sel. Topics Power Electron.*, early access, Mar. 4, 2020, doi: 10.1109/JESTPE.2020.2978262.
[64] L. Liu, Z. Liu, M. Popov, P. Palensky, and M. Van Der Meijden, "A fast protection of multi-terminal HVDC system based on transient signal detection," *IEEE Trans. Power Del.*, early access, Mar. 10, 2020, doi: 10.1109/TPWRD.2020.2979811.
[65] D. Li, A. Ukil, K. Satpathi, and Y. M. Yeap, "Improved s transform based fault detection method in VSC interfaced DC system," *IEEE Trans. Ind. Electron.*, early access, Apr. 21, 2020, doi: 10.1109/TIE.2020.2988193.
[66] L. Sabug, A. Musa, F. Costa, and A. Monti, "Real-time boundary wavelet transform-based DC fault protection system for MTDC grids," *Int. J. Electr. Power Energy Syst.*, vol. 115, Feb. 2020, Art. no. 105475.
[67] X. Chu, G. Song, and J. Liang, "Analytical method of fault characteristic and non-unit protection for HVDC transmission lines," *CSEE J. Power Energy Syst.*, vol. 2, no. 4, pp. 37–43, Dec. 2016.
[68] Y. Li, J. Li, L. Xiong, X. Zhang, and Z. Xu, "DC fault detection in meshed MTdc systems based on transient average value of current," *IEEE Trans. Ind. Electron.*, vol. 67, no. 3, pp. 1932–1943, Mar. 2020.
[69] B. Li, Y. Li, J. He, and W. Wen, "A novel single-ended Transient-Voltage-Based protection strategy for flexible DC grid," *IEEE Trans. Power Del.*, vol. 34, no. 5, pp. 1925–1937, Oct. 2019.
[70] Q. Huai, K. Liu, L. Qin, X. Liao, S. Zhu, Y. Li, and H. Ding, "Backup-protection scheme for multi-terminal HVDC system based on Wavelet-Packet-Energy entropy," *IEEE Access*, vol. 7, pp. 49790–49803, 2019.
[71] Q. Yang, S. Le Blond, R. Aggarwal, Y. Wang, and J. Li, "New ANN method for multi-terminal HVDC protection relaying," *Electr. Power Syst. Res.*, vol. 148, pp. 192–201, Jul. 2017.
[72] Y. Wang, Z. Hao, B. Zhang, and F. Kong, "A pilot protection scheme for transmission lines in VSC-HVDC grid based on similarity measure of traveling waves," *IEEE Access*, vol. 7, pp. 7147–7158, 2019.
[73] A. Raza, A. Akhtar, M. Jamil, G. Abbas, S. Omer Gilani, L. Yuchao, M. Nasir Khan, T. Izhar, X. Dianguo, and B. W. Williams, "A protection scheme for multi-terminal VSC-HVDC transmission systems," *IEEE Access*, vol. 6, pp. 3159–3166, 2018.
[74] J. Li, Y. Li, L. Xiong, K. Jia, and G. Song, "DC fault analysis and transient average current based fault detection for radial MTDC system," *IEEE Trans. Power Del.*, vol. 35, no. 3, pp. 1310–1320, Jun. 2020.
[75] B. Li, M. Lv, B. Li, S. Xue, and W. Wen, "Research on an improved protection principle based on differential voltage traveling wave for VSC-HVDC transmission lines," *IEEE Trans. Power Del.*, vol. 35, no. 5, pp. 2319–2328, Oct. 2020.
[76] D. Tzelepis, A. Dysko, G. Fusiek, J. Nelson, P. Niewczas, D. Vozikis, P. Orr, N. Gordon, and C. D. Booth, "Single-ended differential protection in MTDC networks using optical sensors," *IEEE Trans. Power Del.*, vol. 32, no. 3, pp. 1605–1615, Jun. 2017.
[77] M. Farshad, "A pilot protection scheme for transmission lines of half-bridge MMC-HVDC grids using cosine distance criterion," *IEEE Trans. Power Del.*, early access, Jun. 11, 2020, doi: 10.1109/TPWRD.2020.3001878.
[78] R. Bertho, V. A. Lacerda, R. M. Monaro, J. C. M. Vieira, and D. V. Coury, "Selective nonunit protection technique for multiterminal VSC-HVDC grids," *IEEE Trans. Power Del.*, vol. 33, no. 5, pp. 2106–2114, Oct. 2018.
[79] N. Johannesson and S. Norrga, "Longitudinal differential protection based on the universal line model," in *Proc. 41st Annu. Conf. IEEE Ind. Electron. Soc. (IECON)*, Nov. 2015, pp. 001091–001096.
[80] J. Sneath and A. D. Rajapakse, "Fault detection and interruption in an earthed HVDC grid using ROCOV and hybrid DC breakers," *IEEE Trans. Power Del.*, vol. 31, no. 3, pp. 973–981, Jun. 2016.
[81] R. Li, L. Xu, and L. Yao, "DC fault detection and location in meshed multiterminal HVDC systems based on DC reactor voltage change rate," *IEEE Trans. Power Del.*, vol. 32, no. 3, pp. 1516–1526, Jun. 2017.
[82] N. M. Haleem and A. D. Rajapakse, "Application of new directional logic to improve DC side fault discrimination for high resistance faults in HVDC grids," *J. Mod. Power Syst. Clean Energy*, vol. 5, no. 4, pp. 560–573, Jul. 2017.
[83] L. Tang and B.-T. Ooi, "Locating and isolating DC faults in multi-terminal DC systems," *IEEE Trans. Power Del.*, vol. 22, no. 3, pp. 1877–1884, Jul. 2007.
[84] J. Wang, B. Berggren, K. Linden, and J. Pan, *Multi-Terminal DC System Line Protection Requirement and High Speed Protection Solutions*. Paris, France: CIGRE, 2015, pp. 1–9.
[85] K. De Kerf, K. Srivastava, M. Reza, D. Bekaert, S. Cole, D. Van Hertem, and R. Belmans, "Wavelet-based protection strategy for DC faults in multi-terminal VSC HVDC systems," *IET Gener., Transmiss., Distrib.*, vol. 5, no. 4, pp. 496–503, Apr. 2011.
[86] C. Li, A. M. Gole, and C. Zhao, "A fast DC fault detection method using DC reactor voltages in HVdc grids," *IEEE Trans. Power Del.*, vol. 33, no. 5, pp. 2254–2264, Oct. 2018.
[87] W. Leterme and D. Van Hertem, "Cable protection in HVDC grids employing distributed sensors and proactive HVDC breakers," *IEEE Trans. Power Del.*, vol. 33, no. 4, pp. 1981–1990, Aug. 2018.
[88] R. Dantas, J. Liang, C. E. Ugalde-Loo, A. Adamczyk, C. Barker, and R. Whitehouse, "Progressive fault isolation and grid restoration strategy for MTDC networks," *IEEE Trans. Power Del.*, vol. 33, no. 2, pp. 909–918, Apr. 2018.
[89] S. Wang, C. Li, O. D. Adeuyi, G. Li, C. E. Ugalde-Loo, and J. Liang, "Coordination of MMCs with hybrid DC circuit breakers for HVDC grid protection," *IEEE Trans. Power Del.*, vol. 34, no. 1, pp. 11–22, Feb. 2019.
[90] M. Hajian, L. Zhang, and D. Jovcic, "DC transmission grid with low-speed protection using mechanical DC circuit breakers," *IEEE Trans. Power Del.*, vol. 30, no. 3, pp. 1383–1391, Jun. 2015.
[91] M. Monadi, M. A. Zamani, C. Koch-Ciobotaru, J. I. Candela, and P. Rodriguez, "A communication-assisted protection scheme for direct-current distribution networks," *Energy*, vol. 109, pp. 578–591, Aug. 2016.
[92] S. Pirooz Azad, W. Leterme, and D. Van Hertem, "Fast breaker failure backup protection for HVDC grids," *Electr. Power Syst. Res.*, vol. 138, pp. 99–105, Sep. 2016.

[93] S. Yang, W. Xiang, R. Li, X. Lu, W. Zuo, and J. Wen, "An improved DC fault protection algorithm for MMC HVDC grids based on modal domain analysis," *IEEE J. Emerg. Sel. Topics Power Electron.*, vol. 8, no. 4, pp. 4086–4099, Dec. 2020, doi: 10.1109/JESTPE.2019.2945200.

[94] S. Li, W. Chen, X. Yin, D. Chen, and Y. Teng, "A novel integrated protection for VSC-HVDC transmission line based on current limiting reactor power," *IEEE Trans. Power Del.*, vol. 35, no. 1, pp. 226–233, Feb. 2020.

[95] O. M. K. K. Nanayakkara, A. D. Rajapakse, and R. Wachal, "Traveling-Wave-Based line fault location in star-connected multiterminal HVDC systems," *IEEE Trans. Power Del.*, vol. 27, no. 4, pp. 2286–2294, Oct. 2012.

[96] O. M. K. K. Nanayakkara, A. D. Rajapakse, and R. Wachal, "Location of DC line faults in conventional HVDC systems with segments of cables and overhead lines using terminal measurements," *IEEE Trans. Power Del.*, vol. 27, no. 1, pp. 279–288, Jan. 2012.

[97] D. Wang and M. Hou, "Travelling wave fault location algorithm for LCC-MMC-MTDC hybrid transmission system based on Hilbert-huang transform," *Int. J. Electr. Power Energy Syst.*, vol. 121, Oct. 2020, Art. no. 106125.

[98] S. Azizi, M. Sanaye-Pasand, M. Abedini, and A. Hassani, "A Traveling-Wave-Based methodology for wide-area fault location in multiterminal DC systems," *IEEE Trans. Power Del.*, vol. 29, no. 6, pp. 2552–2560, Dec. 2014.

[99] J. Liu, J. Duan, H. Lu, and Y. Sun, "Fault location method based on EEMD and traveling-wave speed characteristics for HVDC transmission lines," *J. Power Energy Eng.*, vol. 03, no. 04, pp. 106–113, 2015.

[100] P. Chen, B. Xu, J. Li, and Y. Ge, "Modern travelling wave based fault location techniques for HVDC transmission lines," *Trans. Tianjin Univ.*, vol. 14, no. 2, pp. 139–143, Apr. 2008.

[101] M. Ashouri, F. F. da Silva, and C. L. Bak, "On the application of modal transient analysis for online fault localization in HVDC cable bundles," *IEEE Trans. Power Del.*, vol. 35, no. 3, pp. 1365–1378, Jun. 2020.

[102] L. Yuansheng, W. Gang, and L. Haifeng, "Time-domain fault-location method on HVDC transmission lines under unsynchronized two-end measurement and uncertain line parameters," *IEEE Trans. Power Del.*, vol. 30, no. 3, pp. 1031–1038, Jun. 2015.

[103] A. Hadaeghi, H. Samet, and T. Ghanbari, "Multi extreme learning machine approach for fault location in multi-terminal high-voltage direct current systems," *Comput. Electr. Eng.*, vol. 78, pp. 313–327, Sep. 2019.

[104] H. Livani and C. Y. Evrenosoglu, "A single-ended fault location method for segmented HVDC transmission line," *Electr. Power Syst. Res.*, vol. 107, pp. 190–198, Feb. 2014.

[105] Z.-Y. He, K. Liao, X.-P. Li, S. Lin, J.-W. Yang, and R.-K. Mai, "Natural frequency-based line fault location in HVDC lines," *IEEE Trans. Power Del.*, vol. 29, no. 2, pp. 851–859, Apr. 2014.

[106] S. Lan, M.-J. Chen, and D.-Y. Chen, "A novel HVDC double-terminal non-synchronous fault location method based on convolutional neural network," *IEEE Trans. Power Del.*, vol. 34, no. 3, pp. 848–857, Jun. 2019.

[107] D. Tzelepis, S. Mirsaeidi, A. Dysko, Q. Hong, J. He, and C. Booth, "Intelligent fault location in MTDC networks by recognising patterns in hybrid circuit breaker currents during fault clearance process," *IEEE Trans. Ind. Informat.*, early access, Jun. 18, 2020, doi: 10.1109/TII.2020.3003476.

[108] M. Farshad and J. Sadeh, "A novel fault-location method for HVDC transmission lines based on similarity measure of voltage signals," *IEEE Trans. Power Del.*, vol. 28, no. 4, pp. 2483–2490, Oct. 2013.

[109] J. Xu, Y. Lu, C. Zhao, and J. Liang, "A model-based DC fault location scheme for multi-terminal MMC-HVDC systems using a simplified transmission line representation," *IEEE Trans. Power Del.*, vol. 35, no. 1, pp. 386–395, Feb. 2020.

[110] G. Song, T. Wang, and K. S. T. Hussain, "DC line fault identification based on pulse injection from hybrid HVDC breaker," *IEEE Trans. Power Del.*, vol. 34, no. 1, pp. 271–280, Feb. 2019.

[111] J. Suonan, S. Gao, G. Song, Z. Jiao, and X. Kang, "A novel fault-location method for HVDC transmission lines," *IEEE Trans. Power Del.*, vol. 25, no. 2, pp. 1203–1209, Apr. 2010.

[112] D. Tzelepis, A. Dyśko, G. Fusiek, P. Niewczas, S. Mirsaeidi, C. Booth, and X. Dong, "Advanced fault location in MTDC networks utilising optically-multiplexed current measurements and machine learning approach," *Int. J. Electr. Power Energy Syst.*, vol. 97, pp. 319–333, Apr. 2018.

[113] X. Zhang, N. Tai, Y. Wang, and J. Liu, "EMTR-based fault location for DC line in VSC-MTDC system using high-frequency currents," *IET Gener., Transmiss. Distrib.*, vol. 11, no. 10, pp. 2499–2507, Jul. 2017.

[114] J. M. Johnson and A. Yadav, "Complete protection scheme for fault detection, classification and location estimation in HVDC transmission lines using support vector machines," *IET Sci., Meas. Technol.*, vol. 11, no. 3, pp. 279–287, May 2017.

[115] TRENCH. *Resistive Capacitive Voltage Dividers for Gas Insulated Switchgear*. Accessed: Jun. 5, 2017. [Online]. Available: http://www.trenchgroup.com/content/download/1401/11741/file/GIS%20RC20%Voltage%20Divider.pdf

[116] SIEMENS, "Power engineering guide—Answers for energy," Siemens Aktiengesellschaft—Energy Sector, Munich, Germany, Tech. Rep. Edition 7.1, 2014.

[117] K. Schon, *High Impulse Voltage and Current Measurement Techniques*. Berlin, Germany: Springer, 2013.

[118] F. Jenau and G. Testin, "Modern instrument transformer technologies for UHV AC and HVDC networks," in *Proc. 2nd Int. Symp. Standards Ultra High Voltage Transmiss.*, 2009, pp. 1–16.

[119] F. Long, J. Zhang, C. Xie, and Z. Yuan, "Application of the pockels effect to high voltage measurement," in *Proc. 8th Int. Conf. Electron. Meas. Instrum.*, Aug. 2007, p. 495.

[120] A. Kumada and K. Hidaka, "Directly high-voltage measuring system based on pockels effect," *IEEE Trans. Power Del.*, vol. 28, no. 3, pp. 1306–1313, Jul. 2013.

[121] J. C. Santos, M. C. Taplamacioglu, and K. Hidaka, "Pockels high-voltage measurement system," *IEEE Trans. Power Del.*, vol. 15, no. 1, pp. 8–13, Jan. 2000.

[122] Y. Zhang, X. Xiao, and X. Yan, "Review of research on measurement technologies of DC high voltage," in *Proc. 7th Int. Conf. Inf. Technol. Electr. Eng. (ICITEE)*, Oct. 2015, pp. 179–183.

[123] F. Costa, P. Poulichet, F. Mazaleyrat, and E. Labouré, "The current sensors in power electronics, a review," *EPE J.*, vol. 11, no. 1, pp. 7–18, Feb. 2001.

[124] Y. Zhang, Y. Ma, and F. Xing, "A prototype optical fibre direct current sensor for HVDC system," *Trans. Inst. Meas. Control*, vol. 38, no. 1, pp. 55–61, Jan. 2016.

[125] X. Han, Y. Xu, C. Fu, and H. Rao, "Research about measurement performance of optic-electric DC current transformer in 500kV HVDC power system," in *Proc. Asia–Pacific Power Energy Eng. Conf.*, Mar. 2009, pp. 1–4.

[126] R. Han, T. Wang, Q. Wang, Y. Zheng, and L. Dong, "Analysis for measurement errors of DC current sensor in HVDC based on finite element method," in *Proc. IEEE PES Asia–Pacific Power Energy Eng. Conf. (APPEEC)*, Oct. 2016, pp. 1354–1358.

[127] F. Pan, Y. Xu, X. Xiao, K. Xu, and S. Ren, "Characteristic analysis of shunt for high voltage direct current measurement," *Measurement*, vol. 45, no. 3, pp. 597–603, Apr. 2012.

[128] S. Ziegler, R. C. Woodward, H. H.-C. Iu, and L. J. Borle, "Current sensing techniques: A review," *IEEE Sensors J.*, vol. 9, no. 4, pp. 354–376, Apr. 2009.

[129] D. F. Antony, Q. Zhengting, K. Satpathi, N. Thukral, and A. Ukil, "Suitability of rogowski coil for DC shipboard protection," in *Proc. IEEE Region 10 Conf. (TENCON)*, Nov. 2016, pp. 818–822.

[130] Y. Kuwabara, K. Wada, J.-M. Guichon, J.-L. Schanen, and J. Roudet, "Implementation and performance of a current sensor for a laminated bus bar," *IEEE Trans. Ind. Appl.*, vol. 54, no. 3, pp. 2579–2587, May 2018.

[131] K. Hasegawa, S. Takahara, S. Tabata, M. Tsukuda, and I. Omura, "A new output current measurement method with tiny PCB sensors capable of being embedded in an IGBT module," *IEEE Trans. Power Electron.*, vol. 32, no. 3, pp. 1707–1712, Mar. 2017.

[132] TAMURA. *Tamura Closed Loop Hall Effect Current Sensors*. Accessed: Feb. 22, 2019. [Online]. Available: https://www.tamuracorp.com/electronics/en/currentsensors/

[133] LEM. (2004). *Isolated Current and Voltage Transducers: Characteristics–Applications–Calculations*. Accessed: Feb. 22, 2019. [Online]. Available: https://www.lem.com/ru/file/3139/download

[134] J. Lenz and S. Edelstein, "Magnetic sensors and their applications," *IEEE Sensors J.*, vol. 6, no. 3, pp. 631–649, Jun. 2006.

[135] T. P. White, S. Shetty, M. E. Ware, H. A. Mantooth, and G. J. Salamo, "AlGaN/GaN micro-Hall effect devices for simultaneous current and temperature measurements from line currents," *IEEE Sensors J.*, vol. 18, no. 7, pp. 2944–2951, Apr. 2018.

[136] L. Ghislanzoni and J. A. Carrasco, "A DC current transformer for large bandwidth and high common-mode rejection," *IEEE Trans. Ind. Electron.*, vol. 46, no. 3, pp. 631–636, Jun. 1999.

[137] H. C. Appelo, M. Groenenboom, and J. Lisser, "The zero-flux DC current transformer a high precision bipolar wide-band measuring device," *IEEE Trans. Nucl. Sci.*, vol. 24, no. 3, pp. 1810–1811, Jun. 1977.

[138] T. Funk and B. Wicht, "A fully integrated DC to 75 MHz current sensing circuit with on-chip rogowski coil," in *Proc. IEEE Custom Integr. Circuits Conf. (CICC)*, Apr. 2018, pp. 1–4.

[139] P. Ripka, K. Draxler, and R. Styblíková, "DC-compensated current transformer," *Sensors*, vol. 16, no. 1, p. 114, Jan. 2016.

[140] N. Wang, Z. Zhang, Z. Li, Q. He, F. Lin, and Y. Lu, "Design and characterization of a low-cost self-oscillating fluxgate transducer for precision measurement of high-current," *IEEE Sensors J.*, vol. 16, no. 9, pp. 2971–2981, May 2016.

[141] G. Rietveld, J. H. N. van der Beek, and E. Houtzager, "Accurate DC current ratio measurements for primary currents up to 600 a," *IEEE Trans. Instrum. Meas.*, vol. 64, no. 11, pp. 3055–3061, Nov. 2015.

[142] S. J. Nibir, H. Niakan, and B. Parkhideh, "Characterization of magnetoresistors for contactless current sensing in power electronic applications," in *Proc. IEEE Energy Convers. Congr. Exposit. (ECCE)*, Oct. 2017, pp. 433–438.

[143] A. Bernieri, L. Ferrigno, M. Laracca, and A. Rasile, "An AMR-based three-phase current sensor for smart grid applications," *IEEE Sensors J.*, vol. 17, no. 23, pp. 7704–7712, Dec. 2017.

[144] D. F. Wang, H. Liu, X. Li, Y. Li, W. Xian, T. Kobayashi, T. Itoh, and R. Maeda, "Passive MEMS DC electric current sensor: Part I—Theoretical considerations," *IEEE Sensors J.*, vol. 17, no. 5, pp. 1230–1237, Mar. 2017.

[145] D. F. Wang, H. Liu, X. Li, Y. Li, W. Xian, T. Kobayashi, T. Itoh, and R. Meada, "Passive MEMS DC electric current sensor: Part II–experimental verifications," *IEEE Sensors J.*, vol. 17, no. 5, pp. 1238–1245, Mar. 2017.

[146] M. Biglarbegian, S. J. Nibir, H. Jafarian, and B. Parkhideh, "Development of current measurement techniques for high frequency power converters," in *Proc. IEEE Int. Telecommun. Energy Conf. (INTELEC)*, Oct. 2016, pp. 1–7.

[147] C. Reig, M.-D. Cubells-Beltran, and D. R. Munoz, "Magnetic field sensors based on giant magnetoresistance (GMR) technology: Applications in electrical current sensing," *Sensors*, vol. 9, no. 10, pp. 7919–7942, 2009.

[148] R. Weiss, R. Mattheis, and G. Reiss, "Advanced giant magnetoresistance technology for measurement applications," *Meas. Sci. Technol.*, vol. 24, no. 8, Jul. 2013, Art. no. 082001.

[149] N. Tröster, T. Eisenhardt, M. Zehelein, J. Wölfle, J. Ruthardt, and J. Roth-Stielow, "Improvements of a coaxial current sensor with a wide bandwidth based on the HOKA principle," in *Proc. 20th Eur. Conf. Power Electron. Appl. (EPE ECCE Europe)*, Sep. 2018, pp. 1–9.

[150] R. M. Silva, H. Martins, I. Nascimento, J. M. Baptista, A. L. Ribeiro, J. L. Santos, P. Jorge, and O. Frazão, "Optical current sensors for high power systems: A review," *Appl. Sci.*, vol. 2, no. 3, pp. 602–628, Jul. 2012.

[151] J. Blake, P. Tantaswadi, and R. T. de Carvalho, "In-line sagnac interferometer current sensor," *IEEE Trans. Power Del.*, vol. 11, no. 1, pp. 116–121, Jan. 1996.

[152] M. Takahashi, K. Sasaki, Y. Hirata, T. Murao, H. Takeda, Y. Nakamura, T. Ohtsuka, T. Sakai, and N. Nosaka, "Field test of DC optical current transformer for HVDC link," in *Proc. IEEE PES Gen. Meeting*, Jul. 2010, pp. 1–6.

[153] ABB. *Review: Light Measures Current*. Accessed: Feb. 10, 2019. [Online]. Available: https://library.e.abb.com/public/0d948cedb40451cec1257ca900532dd0/12-17%201m411_EN_72dpi.pdf

[154] K. Bohnert, H. Brandle, M. G. Brunzel, P. Gabus, and P. Guggenbach, "Highly accurate fiber-optic DC current sensor for the electrowinning industry," *IEEE Trans. Ind. Appl.*, vol. 43, no. 1, pp. 180–187, Jan. 2007.

[155] ABB. *FOCS–Fibre-Optic Current Sensor*. Accessed: Jun. 6, 2017. [Online]. Available: https://library.e.abb.com/public/74d5555d2a9c2998c12579a00038ff0a/FOCS_brochure_3BHS362996_E01.pdf

[156] N. Phase. *Optical CTs and VTs*. Accessed: Feb. 24, 2019. [Online]. Available: http://www.saiceemg.com/tva/uploads/Nxt-Sensor-Brochure.pdf

[157] GE Grid Solutions. *COSI-CT F3 Flexible Optical Current Transformer*. Accessed: Feb. 24, 2019. [Online]. Available: https://www.gegridsolutions.com/app/Resources.aspx?prod=cosi&type=1

[158] GE Grid Solutions. *COSI-CT Optical Current Transformer*. Accessed: Feb. 24, 2019. [Online]. Available: https://www.gegridsolutions.com/products/brochures/Grid-GA-L3-COSI_CT-0907-2016_07-EN.pdf

[159] J. Blake and A. Rose, "Interfacing optical CTs and VTs to relays and meters," in *Proc. IEEE/PES Transmiss. Distrib. Conf. Exhib.*, May 2006, pp. 1280–1284.

[160] S. Kucuksari and G. G. Karady, "Experimental comparison of conventional and optical current transformers," *IEEE Trans. Power Del.*, vol. 25, no. 4, pp. 2455–2463, Oct. 2010.

[161] D. Peelo, F. Rahmatian, M. Nagpal, and D. Sydor, "Real-time monitoring and capture of power system transients," in *Proc. CIGRE*, Paris, France, Aug. 2012, pp. 1–8.

[162] F. V. B. de Nazare and M. M. Werneck, "Compact optomagnetic Bragg-Grating-Based current sensor for transmission lines," *IEEE Sensors J.*, vol. 15, no. 1, pp. 100–109, Jan. 2015.

[163] R. L. Heredero, J. L. Santos, R. Fernandez de Caleya, and H. Guerrero, "Micromachined low-finesse Fabry–Pérot interferometer for the measurement of DC and AC electrical currents," *IEEE Sensors J.*, vol. 3, no. 1, pp. 13–18, Feb. 2003.

[164] F. Jenau and G. Testin, "Modern instrument transformer technologies for uhv ac and hvdc networks," *Water Energy Int.*, vol. 66, no. 2, pp. 31–42, Apr. 2009.

[165] Corning-Inc. *SMF-28 Ultra Optical Fiber*. Accessed: Oct. 25, 2016. [Online]. Available: https://www.corning.com/media/worldwide/coc/documents/Fiber/SMF-2820Ultra.pdf

[166] L. Dziuda, P. Niewczas, G. Fusiek, and J. R. McDonald, "Hybrid fiber optic voltage sensor for remote monitoring of electrical submersible pump motors," *Opt. Eng.*, vol. 44, no. 6, Jun. 2005, Art. no. 064401.

[167] L. Dziuda, G. Fusiek, P. Niewczas, G. M. Burt, and J. R. McDonald, "Laboratory evaluation of the hybrid fiber-optic current sensor," *Sens. Actuators A, Phys.*, vol. 136, no. 1, pp. 184–190, May 2007.

[168] D. Reilly, A. J. Willshire, G. Fusiek, P. Niewczas, and J. R. McDonald, "A Fiber-Bragg-Grating-Based sensor for simultaneous AC current and temperature measurement," *IEEE Sensors J.*, vol. 6, no. 6, pp. 1539–1542, Dec. 2006.

[169] G. Fusiek and P. Niewczas, "Preliminary characterization of an optical current sensor for HVDC networks," in *Proc. IEEE Int. Instrum. Meas. Technol. Conf. (I2MTC)*, 2018, pp. 1–5.

[170] G. Fusiek, P. Niewczas, and J. R. McDonald, "Feasibility study of the application of optical voltage and current sensors and an arrayed waveguide grating for aero-electrical systems," *Sens. Actuators A, Phys.*, vol. 147, no. 1, pp. 177–182, Sep. 2008.

[171] *Instrument Transformers-Part 1: General Requirements*, BSI, London, U.K., document IEC 61869-ED 1.0, 2007.

[172] *Instrument Transformers-Part 6: Additional General Requirements for Low-Power Instrument Transformers*, BSI, London, U.K., document IEC 61869-ED 1.0, 2016.

[173] *Instrument Transformers–Part 14: Specific Requirements for DC Current Transformers*, BSI, London, U.K., document IEC 61869-14: ED 1.0, 2014.

[174] *Instrument Transformers–Part 15: Specific Requirements for DC Voltage Transformers*, BSI, London, U.K., document IEC 61869-15: ED 1.0, 2014.

[175] *Instrument Transformers–Part 14: Additional Requirements for Current Transformers for DC Applications*, BSI, London, U.K., document IEC 61869-14: ED 1.0, 2018.

[176] *Instrument Transformers–Part 15: Additional Requirements for Voltage Transformers for DC Applications*, BSI, London, U.K., document IEC 61869-15: ED 1.0, 2018.

[177] *Instrument Transformers–Part 7: Electronic Voltage Transformers*, BSI, London, U.K., document IEC 60044:7, Dec. 1999.

[178] *Instrument Transformers–Part 10: Additional Requirements for Low-Power Passive Current Transformers*, BSI, London, U.K., document IEC 61869-10: ED 1.0, 2017.

[179] *Instrument Transformers–Part 11: Additional Requirements for Low-Power Passive Voltage Transformers*, BSI, London, U.K., document IEC 61869-11: ED 1.0, 2017.

[180] D. Tzelepis, H. Ha, S. Subramanian, A. Dysko, S. Ademi, and D. Vozikis, "Impact of VSC converter topology on fault characteristics in HVDC transmission systems," in *Proc. 8th IET Int. Conf. Power Electron., Mach. Drives (PEMD)*, 2016, p. 6.

[181] *Communication Networks and Systems in Substations. Specific Communication Service Mapping (SCSM). Sampled Values Over Serial Unidirectional Multidrop Point to Point Link*, BSI, London, U.K., document IEC 61850-9-1:2003, 2003.
[182] *Communication Networks and Systems for Power Utility Automation. Part 9–2: Specific Communication Service Mapping (SCSM)–Sampled Values Over ISO/IEC 8802-3 View Details*, BSI, London, U.K., document IEC 61850-9-2:2011+a1:2020, Feb. 2012.
[183] *IEEE Recommended Practice for Implementing an IEC 61850-Based Substation Communications, Protection, Monitoring, and Control System*, IEEE Standard 2030.100-2017, Jun. 2017, pp. 1–67.
[184] *Teleprotection Equipment of Power Systems–Performance and Testing Command Systems*, BSI, London, U.K., document IEC 60834-1:2000, Aug. 2000.
[185] *Industrial Communication Networks. High Availability Automation Networks. Parallel Redundancy Protocol (PRP) and High-Availability Seamless Redundancy (HSR)*, BSI, London, U.K., document IEC 62439-3:2018–TC, Feb. 2020.
[186] *Power Systems Management and Associated Information Exchange. Data and Communications Security. Role-Based Access Control for Power System Management*, BSI, London, U.K., document IEC 62351-8:2020, Jul. 2020.
[187] *Communication Networks and Systems for Power Utility Automation—Part 90–14: Using IEC 61850 for FACTS (Flexible AC Transmission Systems), HVDC (High Voltage Direct Current) Transmission and Power Conversion Data Modelling*, document 57/2273/RVDTR, BSI, 2021.
[188] B. Li, Y. Li, J. He, B. Li, S. Liu, B. Liu, and L. Xu, "An improved transient traveling-wave based direction criterion for multi-terminal HVDC grid," *IEEE Trans. Power Del.*, vol. 35, no. 5, pp. 2517–2529, Oct. 2020.
[189] N. Johannesson and S. Norrga, "Sensitivity of cable model parameters for traveling wave differential protections in MTDC systems," *IEEE Trans. Power Del.*, vol. 35, no. 5, pp. 2212–2221, Oct. 2020.
[190] *IEEE Guide for Determining Fault Location on AC Transmission and Distribution Lines*, IEEE Standard C37.114-2014, Jan. 2015, pp. 1–128.
[191] C.-K. Jung, H.-S. Park, J.-W. Kang, X. Wang, Y.-K. Kim, and J.-B. Lee, "Development of fault location algorithm and its verification experiments for HVDC submarine cables," *J. Electr. Eng. Technol.*, vol. 7, no. 6, pp. 859–868, Nov. 2012.
[192] G.-Y. Kwon, C.-K. Lee, G. Seok Lee, Y. Ho Lee, S. Jin Chang, C.-K. Jung, J.-W. Kang, and Y.-J. Shin, "Offline fault localization technique on HVDC submarine cable via time–frequency domain reflectometry," *IEEE Trans. Power Del.*, vol. 32, no. 3, pp. 1626–1635, Jun. 2017.
[193] M. Bawart, M. Marzinotto, and G. Mazzanti, "Diagnosis and location of faults in submarine power cables," *IEEE Elect. Insul. Mag.*, vol. 32, no. 4, pp. 24–37, Jul. 2016.

DIMITRIOS TZELEPIS (Member, IEEE) received the B.Eng. degree (Hons.) in electrical engineering from the Technological Education Institution of Athens, Athens, Greece, in 2013, and the M.Sc. degree in wind energy systems and the Ph.D. degree from the University of Strathclyde, Glasgow, U.K., in 2014 and 2017, respectively. He is currently a Postdoctoral Researcher with the Department of Electronic and Electrical Engineering, University of Strathclyde. His research interests include power system protection, automation and control of future electricity grids, incorporating increased penetration of renewable energy sources, and high voltage direct current interconnections. His main research methods include implementation of intelligent algorithms for protection, fault location and control applications, including the utilisation of machine learning methods and advanced and intelligent signal processing techniques. He is also interested in the application, control and protection of hybrid AC/DC grids including super-conducting feeders, non-homogeneous transmission lines, and advanced sensing technologies. Additionally, he is investigating potential solutions towards the optimised performance of active distribution networks both in off-grid and on-grid modes, to facilitate a wide suite of grid services and control capabilities.

VASILEIOS PSARAS (Student Member, IEEE) received the diploma degree in electrical engineering from the University of Patras, Patras, Greece, in 2014, and the M.Sc. degree in wind energy systems from the University of Strathclyde, Glasgow, U.K., in 2016, where he is currently pursuing the Ph.D. degree with the Department of Electronic and Electrical Engineering. His research interests include DC grid protection, fault location, and advanced signal analysis for protection applications.

ELENI TSOTSOPOULOU (Student Member, IEEE) received the M.E. degree in electrical and computer engineering from the Democritus University of Thrace, Greece, in 2018, and the M.Sc. degree in wind energy systems from the University of Strathclyde, Glasgow, U.K., in 2019, where she is currently pursuing the Ph.D. degree with the Department of Electronic and Electrical Engineering. Her research interests include power system protection, relay algorithms, integration of distributed generation, and applied superconductivity.

SOHRAB MIRSAEIDI (Member, IEEE) received the Ph.D. degree in electrical engineering from Universiti Teknologi Malaysia (UTM), Malaysia, in 2016. He furthered his Postdoctoral Fellowship at the Department of Electrical Engineering, Tsinghua University, China, from 2016 to 2019. He is currently an Associate Professor with the School of Electrical Engineering, Beijing Jiaotong University, China. He has authored more than 50 articles and two books in the field of microgrids and large-scale power systems, and has been involved in several national research projects in China. His research interests include control and protection of large-scale hybrid AC/DC grids and microgrids, power system stability, and application of power electronics in power systems. He is also a member of IET, CIGRE, and Chinese Society of Electrical Engineering (CSEE).

ADAM DYŚKO (Member, IEEE) received the Ph.D. degree in electrical and electronic engineering from the University of Strathclyde, Glasgow, U.K., in 1998. He is currently a Senior Lecturer with the Department of Electronic and Electrical Engineering. He teaches a variety of electrical engineering subjects and has been leading several research projects with both academic and industrial partners. His research interests include power system protection, control and stability, and power quality.

QITENG HONG (Member, IEEE) received the B.Eng. (Hons.) and Ph.D. degrees in electronic and electrical engineering from the University of Strathclyde, Glasgow, U.K., in 2011 and 2015, respectively. He is currently a Lecturer (Chancellor's Fellow) with the University of Strathclyde. His research interests include power system protection and control in future networks with low inertia, resulting from high penetration of renewable generation. He is also a Regular Member of the CIGRE Working Group B5.50, the IEEE Working Group P2004, and the Technical Lead with the CIGRE UK Next Generation Network.

XINZHOU DONG (Fellow, IEEE) received the B.Sc., M.Sc., and Ph.D. degrees in electrical engineering from Xian Jiaotong University, China, in 1983, 1991, and 1996, respectively. He was a Postdoctoral Researcher with the Electrical Engineering Station, Tianjin University, Tianjin, China, from 1997 to 1998. Since 1999, he has been with Tsinghua University, Beijing, China, where he is currently a Professor with the Department of Electrical Engineering and the Director of the International Union Research Center of Beijing on Green Energy and Power Safety. He has authored or coauthored over 200 journal articles. His research interests include protective relaying, fault location, and the application of wavelet transforms in power systems. He is also a Fellow of IET.

STEVEN M. BLAIR (Senior Member, IEEE) received the M.Eng. degree (Hons.) in computer and electronic systems and the Ph.D. degree in electrical engineering from the University of Strathclyde, Glasgow, U.K., in 2008 and 2013, respectively. He is currently the Head of Power Systems Technologies, Synaptec Ltd., U.K., and a Lecturer with the Department of Electronic and Electrical Engineering, Institute for Energy and Environment, University of Strathclyde. His research interests include power system protection, communications, measurements, power quality, and real-time simulation. He is also a member of IEC Technical Committee 57 Working Group 10 and the CIGRE Working Group B5.64.

VASSILIS C. NIKOLAIDIS (Senior Member, IEEE) received the five-year Diploma degree in electrical and computer engineering from the Department of Electrical and Computer Engineering, Democritus University of Thrace, Xanthi, Greece, in 2001, and the M.Eng. degree in energy engineering and management and the doctor of engineering degree from the National Technical University of Athens, Athens, Greece, in 2002 and 2007, respectively. Since 2008, he has been a Power Systems Consulting Engineer. He is currently an Assistant Professor with the Department of Electrical and Computer Engineering, Democritus University of Thrace. His research interests include with power system protection, control, stability, and transients.

VASSILIS PAPASPILIOTOPOULOS (Member, IEEE) received the Diploma degree in electrical and computer engineering and the Ph.D. degree from the National Technical University of Athens (NTUA), Greece, in 2012 and 2020, respectively. He is currently a Manager of the Department of Power System Operation Studies & Consulting, PROTASIS SA. His research interests include modern protection methods and optimization techniques in power systems. He is also a member of the IEEE Power & Energy Society (PES), the IEEE Industry Applications Society (IAS), and the Technical Chamber of Greece.

GRZEGORZ FUSIEK (Member, IEEE) received the M.Sc. degree in electrical engineering from the Lublin University of Technology, Poland, in 2000, and the Ph.D. degree in interrogation systems for spectrally encoded sensors from the University of Strathclyde, Glasgow, U.K., in 2007. He is currently a Research Fellow with the Department of Electronic and Electrical Engineering, Institute for Energy and Environment. His research interests include optical sensing techniques for power industry and energy systems applications.

GRAEME M. BURT (Member, IEEE) received the B.Eng. degree in electrical and electronic engineering and the Ph.D. degree in fault diagnostics in power system networks from the University of Strathclyde, Glasgow, U.K., in 1988 and 1992, respectively. He is currently a Distinguished Professor of electrical power systems with the University of Strathclyde, where he directs the Institute for Energy and Environment, directs the Rolls-Royce University Technology Centre in Electrical Power Systems, and is also a Lead Academic for the Power Networks Demonstration Center (PNDC). In addition, he serves on the board of DERlab e.V., the association of distributed energy laboratories. His research interests include decentralised energy and smart grid protection and control, electrification of aerospace and marine propulsion, DC and hybrid power distribution, and experimental systems testing and validation with power hardware in the loop.

PAWEL NIEWCZAS (Member, IEEE) received the M.Sc. degree in electrical engineering from the Technical University of Lublin, in 1995, and the Ph.D. degree in optical current sensors from the University of Strathclyde, Glasgow, in 2000. He is currently a Reader with the Department of Electronic and Electrical Engineering, University of Strathclyde, and Leading the Advanced Sensors Team with the Institute for Energy and Environment, University of Strathclyde. His research interests include the advancement of optical sensing methods in such areas as power system metering and protection, gas turbine monitoring, downhole pressure, temperature, voltage, and current measurement, sensing in nuclear fission and fusion environments, and other sensing applications. He has published over 100 technical articles in the above areas.

CAMPBELL D. BOOTH (Member, IEEE) received the B.Eng. and Ph.D. degrees in electrical and electronic engineering from the University of Strathclyde, Glasgow, U.K., in 1991 and 1996, respectively. He is currently a Professor and the Head of the Department for Electronic and Electrical Engineering, University of Strathclyde. His research interests include power system protection, plant condition monitoring and intelligent asset management, applications of intelligent system techniques to power system monitoring, protection, and control, knowledge management, and decision.